TESIS - TL 142501

Paduan Ternari Basis Pd dengan Kemampuan Reaksi Oksidasi Metanol Tinggi untuk Aplikasi Sel Bahan Bakar Metanol

YUSUF PRADESAR
2714 201 005

DOSEN PEMBIMBING
Diah Susanti, S.T., M.T., Ph.D.
Dr. Chen-Hao Wang

PROGRAM MAGISTER
BIDANG KEAHLIAN TEKNIK KOROSI, METALURGI, DAN MATERIAL INOVATIF
JURUSAN TEKNIK MATERIAL DAN METALURGI
FAKULTAS TEKNOLOOGI INDUSTRI
INSTITUT TEKNOLOGI SEPULUH NOPEMBER
SURABAYA
2016

THESIS - TL 142501

Pd-Based Ternary Alloy Supported Carbon Black with High Methanol Oxidation Reaction for Direct Methanol Fuel Cell Application

YUSUF PRADESAR
2714 201 005

SUPERVISOR
Diah Susanti, S.T., M.T., Ph.D.
Dr. Chen-Hao Wang

MASTER PROGRAM
INOVATIVE MATERIALS
MATERIALS AND METALLURGICAL ENGINEERING
FACULTY OF INDUSTRIAL TECHNOLOGY
SEPULUH NOPEMBER INSTITUTE OF TECNOLOGY
SURABAYA
2016

Pd-BASED TERNARY ALLOY SUPPORTED CARBON BLACK WITH HIGH METHANOL OXIDATION REACTION FOR DIRECT METHANOL FUEL CELL APPLICATION

This thesis is composed with the expectation of getting the approval from Materials and Metallurgical Engineering Graduate Program, supervisor, and committee member of this research to fulfill the requirement for Megister Teknik (M.T) degree

in

Institut Teknologi Sepuluh Nopember Surabaya

Research Execution:

YUSUF PRADESAR

NRP 2714 201 005

Exam Date : July, 19th 2016

Graduation Period : September 2016

Approved by:

1. Dr. Chen-Hao Wang (Supervisor I)
2. Diah Susanti, S.T., M.T., Ph.D (Supervisor II)

   NIP. 197701062003122001
3. Dr. Shao-Ju Shih (Committee I)
4. Dr. Kuan-Wen Wang (Committee II)
5. Dr. Yuan-Chang Liang (Committee III)
6. Dr. Sun-Tang Chang (Committee IV)

Graduate Program Director,

Prof.Ir. Djauhar Manfaat, M.Sc, Ph.D

NIP. 19601202 198701 1 001

ABSTRAK

Suplai energi merupakan kebutuhan mendesak bagi masyarakat di abad 21 ini karena krisis energi fosil yang tidak terbarukan. Sehingga,, pengadaan energi baru yang layak, seperti sel bahan bakar, telah menarik perhatian para peneliti. Sel bahan bakar temperatur rendah sesuai untuk aplikasi kendaraan dan *portable* karena densitas energinya yang tinggi, temperatur kerja rendah, dan rendah emisi polusi. Untuk meningkatkan aktivitas elektrokatalitik katalis mono-Pd, banyak penelitian yang memodifikasi Pd dengan memadukannya. Dalam penelitian ini, karbon hitam XC-72 digunkan sebagai material support dan $Pd(acac)_2$ sebagai precursor logam Pd. Untuk mensintesis elektrokatalis, metode emulsi digunakan sebagai prosedur eksperimen. Benzil alcohol digunakan sebagai larutan dan campuran oleylamine dan asam oleic sebagai reduktor.

Dalam penelitian ini, pengaruh parameter eksperimental diteliti. Rasio antara volume reduktor dengan volume keseluruhan 0.5, 0.3, dan 0.1; dan temeperature reduksi 110, 130, dan 150 ^oC dipilih untuk meningkatkan aktivitas katalitiknya. Faktor lain yang memepengaruhi aktivitas katalitik adalah elemen paduan. Fe, Co, dan Ni digunakan sebagai elemen paduan. Pengujian XRD, SEM dan TEM dilakukan untuk mengetahui sifat fisik elektrokatalis. Pengukuran CV dilakukan untuk mengetahui sifat elektrokimia dalam larutan 1 M KOH dan 1 M KOH + 1 M methanol. Hasil penelitian menunjukkan bahwa volume rasio 0.1 dan temperatur reduksi 150 ^oC merupakan parameter eksperimental terbarik untuk mensisntesis paduan logam ternary basis Pd. PdFeCo/C merupakan paduan logam ternary yang memiliki aktivitas katalitik dan stabilitas terhadap methanol terbaik.

ABSTRACT

Energy supply is an urgent need for society in this 21st century due the crisis of fossil fuels. Therefore, development new feasible energy, such as fuel cells, has drawn research interest. Low temperature fuel cells are suitable for transportation and portable application because of their high energy density, low operation temperature and low pollution emissions. To improve the electrocatalytic activity of mono-Pd catalyst, most of the work has addressed to the modification of Pd environment by alloying with other elements. In this study, XC72 was used as carbon support and $Pd(acac)_2$ as Pd metal precursor. For preparing the electrocalysts, emulsion method was used as experimental procedure. Benzyl alcohol was used as solution, and oleylamine and oleic acid was used as reducing agent and surfactant.

In this study, effect of experimental parameter was studied. Volume ration between reducing agent and total volume 0.5, 0.3, 0.1; and reduction temperature 110, 130, and 150 ºC was considered for improving the catalytic activity. Another factor would affect the catalytic activity was alloying elements. There were Fe, Co, and Ni that used as alloying elements. XRD, SEM, and TEM were conducted to study the physical properties of electrocatalysts. CV measurement was conducted to study the electrochemical properties in 1 M KOH and 1 M KOH + 1 M methanol. The results showed that the volume ratio 0.1 and reduction temperature 150 ºC was the best experimental parameter for synthesized Pd-based ternary alloy. PdFeCo/C was ternary alloy that had the best catalytic activity and good stability toward MOR.

Keywords: DMFC, Pd-based, ternary alloy

TABLE OF CONTENTS

LIST OF TABLES

TABLE OF FIGURES

CHAPTER I
INTRODUCTION

1.1 Research Background

Energy supply is an urgent need for society in this 21st century due the crisis of fossil fuels. Therefore, development new feasible energy, such as fuel cells, has drawn research interest. Low temperature fuel cells are suitable for transportation and portable application because of their high energy density, low operation temperature and low pollution emissions (Yang et al., 2015, Amin et al., 2014, Singh et al., 2009). Fuel cells work by convert chemical energy directly into electrical energy. Direct methanol fuel cell (DMFC) has attracted attention because the high energy density and ease handling liquid fuel (Jeon et al., 2009). DMFC uses methanol and oxygen as anode and cathode reactant, respectively, to produce CO_2, water, and electricity. Compared to hydrogen-fed fuel cells, which have reforming or low capacity in the hydrogen storage tank, DMFC uses a liquid methanol fuel, which easily stored, transported, and simplifies the fuel cell system (Ji et al., 2012). Alkaline DMFC is better than acidic DMFC because reaction dynamics are best facilitate in alkaline media compare in acidic media (Fashedemi et al., 2015).

One of two major challenges in DMFCs is slow anode kinetics that can only overcome by developing new anode catalysts (Liu et al., 2006). The most common used as electrocatalyst are Pt-based catalysts, respectively. The limitation of Pt catalysts comes from high cost and limited resource of Pt, and Pt is easily poisoned by CO. Two effective approach to overcome the limitedness of Pt-based catalysts is reducing the usage of the Pt or replace the Pt catalysts. Pd is a suitable low-cost transition metal for replacing Pt in DMFC. Two main reasons for replacing Pt with Pd are Pd more abundant in nature than Pt and Pd catalysts exhibits better kinetics for DMFC than Pt catalysts. To improve the electrocatalytic activity of mono-Pd catalyst, most of the work has addressed to the modification of Pd environment by alloying with other elements. The additive elements used to alloying with Pd should provide oxygen-containing species at low potential to

oxidize adsorbed CO, such as Ni(Chen et al., 2015c, Lee et al., 2012, Li et al., 2013, Amin et al., 2014, Choi et al., 2013), Fe(Hung et al., 2016), Co(Wang et al., 2014, Qin et al., 2015), Au(Wang et al., 2015, Renjith and Lakshminarayanan, 2015, Maiyalagan et al., 2014), and others. Alloy nanoparticles consisting of Pd and non-noble metals have been considered as the one best alternative electrocatalysts to replace Pt-based catalysts for methanol oxidation reaction (MOR).

Many Pd binary alloy catalysts had been investigated their MOR activity but there are not too many investigations in Pd ternary alloy catalysts. Zhang at al (Zhang et al., 2015c) investigated the MOR activity of mono Pd/RGO, binary CuPd/RGO and FePd/RGO, and ternary CuFePd/RGO. The CV result show that the MOR activity follow this order Pd/RGO < CuPd/RGO < FePd/RGO < CuFePd/RGO. Therefore, ternary alloy will have better MOR activity than binary alloy, because the present of Cu and Fe not only increased the utilization efficiency, but also reduce the CO-like carbonaceous species on the Pd surface, making more active sites available for MOR (Zhang et al., 2015c). With this mind, the Pd based ternary alloy could be applied into anode catalyst for DMFC application and improve the catalytic activity.

1.2 Problem Formulation

The problems were discussed in this work are

1. What is the effect of volume ratio between reductant to total volume on physical and electrochemical characteristic of catalyst?
2. What is the effect of reduction temperature on physical and electrochemical characteristic of catalyst?
3. What is the effect of different alloying metal in the catalytic activity of catalysts?

1.3 Research Objectives

This research focuses on three themes, including

1. Observed the effect of volume ratio between reductant to total volume on physical and electrochemical characteristic of catalyst

2. Observed the effect of reduction temperature on physical and electrochemical characteristic of catalyst
3. Study different alloying metal to improve the catalytic activity

1.4 Research Advantages

Pd based ternary metal can be applied as anode material in DMFC application that has better catalytic activity toward methanol oxidation reaction.

CHAPTER II
LITERATURE REVIEW

2.1 Fuel Cell

Some devices are capable of converting Gibbs energy of the fuel directly into the electricity these are called fuel cells. The advantage of fuel cell is that it not a heat engine and these were not limited by the Carnot efficiency. The concept of the fuel cell arises directly from the operating principle of the electric cell, and as early as 1880, Wilhelm Ostwald realized that chemical process could approach efficiency of 100% in galvanic cells, and these not limited by the Carnot efficiency. Conversion efficiencies as high as 60-80% have been achieved for fuel cells operating in hybrid systems. Another advantage of fuel cell is that its efficiency is not reduce by part load operation, as is the case for all heat engines. Hence, if a fuel operating on hydrocarbon fuels can be developed, it will improve thermal efficiency significantly and reduce pollution by CO_2 and NO_x (Winterbone and Turan, 2015).

As can be note seen from Table 2.1, liquid fuels show a significantly higher combustion energy density than hydrogen in its various forms of storage. It is obvious that long-chain hydrocarbon fuels such as diesel are particularly high in energy density. However, the complete electrochemical oxidation of fuels containing C–C bonds at low potential could not be achieve so far at technically relevant current densities. Therefore, methanol is the most likely option for a fuel cell directly consuming a liquid fuel. (Jorissen and Gogel, 2009)

Table 2.1 Combustion energy density per liter of stored fuel (the values given are based on the lower heating value (LHV)) (Jorissen and Gogel, 2009)

Fuel	Combustion energy density (kW h L^{-1})
Hydrogen pressurized at 200 bar	0.46
Hydrogen pressurized at 350 bar	0.71
Hydrogen pressurized at 700 bar	1.11
Hydrogen liquid	2.35
Methanol	4.44
Ethanol	5.87
Gasoline	~8.8
Diesel	~10

2.2 Direct Methanol Fuel Cell (DMFC)

Hydrogen is the most preferred fuel of fuel cells due to its high reactivity for the anode oxidation reaction and lack of any emission other than pure water. However, hydrogen does not exist naturally as fossil fuels, and so, over 95% of hydrogen is currently produced from fossil sources such as CH_4, NH_3, CH_3OH, C_2H_5OH, C_8H_{18}, etc. These hydrogen sources, therefore, need to go first through fuel processing to convert hydrogen, using different chemical conversion techniques. In this context, the use of hydrogen carriers such as alcohols in a DAFC appears particularly convenient, because they are liquids (allowing easy storage) and their theoretical mass energy densities are rather high (6.1 and 8.0 kWh/kg for CH_3OH and C_2H_5OH, respectively) (Singh et al., 2013).

As a subcategory of proton exchange membrane fuel cells (PEMFCs), direct methanol fuel cells (DMFCs) use methanol as the fuel and directly convert the chemical energy into electric energy without use reformers. DMFC technology can be categorize into two types based on the fuel state to be supplying to the fuel cell: vapor-feed and liquid-feed system. Figure 2.1 shows a simplified schematic of the two DMFC systems (Jorissen and Gogel, 2009). Vapor-feed system allows better electrode kinetics and lower losses owing to less fuel crossover to cathode, but it has some difficulties, such as the thermal management and separation between

the methanol gas and exhausted carbon dioxide. These difficulties hinder the development of this type of system (Zhao and Xu, 2009).

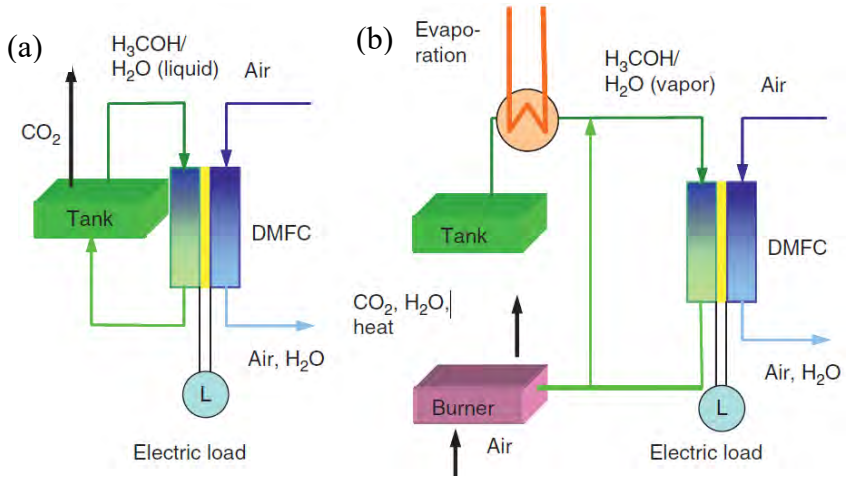

Figure 2.1 Direct methanol fuel cell (DMFC) system design principles: (a) liquid-feed DMFC, (b) vapor-feed DMFC. (Jorissen and Gogel, 2009)

The typical DMFC system operates with the anode being supply with a liquid mixture of methanol and water whereas the cathode is supplying with air. The liquid anode fuel is typically a dilute (1–10 wt%) methanol in water. As methanol consumed, carbon dioxide forms at the anode. Schemes have been developed for venting the carbon dioxide and replenishing the methanol concentration from a pure methanol reservoir using water from the cathode in order to raise the energy content of the system. Water is produce at the cathode. Furthermore, there are significant amounts of water from electroosmotic drag. These also need to be capture and recycle. In order to close the water balance, cooling of the exhaust flow is required. After the water flushed out of the stack by the flow of air through the cathode gas flow channels, pumps and wicks have been developed for recycling the cathode water to the anode to maintain the correct methanol/water mixture by mixing it with a supply of higher concentration methanol (Gervasio, 2009).

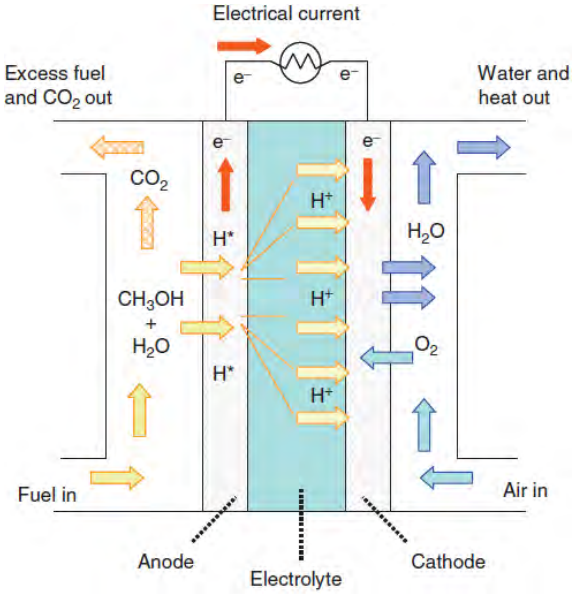

Figure 2.2 Sketch of direct methanol fuel cell. (Gervasio, 2009)

The cell voltage (V_{cell}) is the force that moves the electrons from the anode to the cathode through the external circuit of the fuel cell. The higher the cell voltage at a given current, then the more power the cell can provide. The voltage across the cell (V_{cell}) is the difference between the electrical potential at the anode half-cell side of the fuel cell, due to methanol oxidation ($E_{methanol\ anode}$ = ~ 0 V), and the potential at the cathode half-cell side, due to oxygen reduction ($E_{oxygen\ cathode}$ = ~ 1.2 V). Under ideal conditions, a DMFC will have a cell voltage of

$$V_{Cell} = V_{cathode} - V_{anode} = 1.2 - 0 = 1.2\ V \qquad 2.4$$

This ideal DMFC voltage is a little less than the ideal voltage of a H_2 PEMFC. The operating voltage of the DMFC is not the ideal 1.2 V but is much lower, a result of non-ideal behavior in the fuel cell, such as slow electrode reactions and mixed potentials at the electrodes due to undesirable reactant crossover from one electrode to the other. This DMFC voltage depends mainly on load, temperature, fuel concentration, and the precise materials used, especially the catalyst loading. Typical values of operating voltage for the DMFC are in the region of 0.4 – 0.6 V at current densities of 50 – 200 mA cm^{-2} and at temperatures of 50–110 °C (Gervasio, 2009).

DMFC has some important parts, there are:

2.2.1. Electrolyte Membranes

The polymer electrolyte membranes used in fuel cell have to fulfill the following requirements:

- High ionic conductivity;
- No or very low electronic conductivity
- Stability under the operating and storage conditions (temperature, pressure, flow)
  - Chemical stability with respect to fuel and oxidant
  - Mechanical stability under the application of clamping force; and
- Sufficient low permeability to fuel and oxidant

These requirements apply for H_2 PEMFC as well as for DMFC. Due to the high activity of water at the anode in normal liquid fed DMFCs, there is no driving force for back-diffusion of water, so the cathode is flooded with water from electroosmotic drag causing mass transport issues. In order to keep the losses caused by methanol being transport from the anode to cathode reasonably low, methanol is supplying as a diluted solution in water. Concentrations in the range from 1 mol L^{-1} (~3 wt%) to 4 mol L^{-1} (~12 wt%) are typical for practical applications.

Most commonly used as membrane in DMFC is Nafion, one of the perfluorosulfonic acid (PFSA) membrane. Nafion uses as membrane in DMFC application due to its high proton conductivity and good chemical stability resulting good performance and durability. The proton and water transport properties of Nafion could be well explain by cluster network model shown in Figure 2.3. The hydrophobic polytetrafluoroethylene (PTFE) backbone of PFSA polymers provides thermal and chemical stability and form hydrophobic regions, while the perflurinated side chains terminating with the hydrophilic sulfonic acid groups (-SO_3H) form hydrophilic region (cluster and channels). The clusters formed by the absorbed water and side chains are around 4 nm wide, which are periodically arranged among the hydrophobic region. The distance between the clusters is

around 5.0 nm, and the clusters are connected by channels with a diameter of 1 nm (Manthiram et al., 2012).

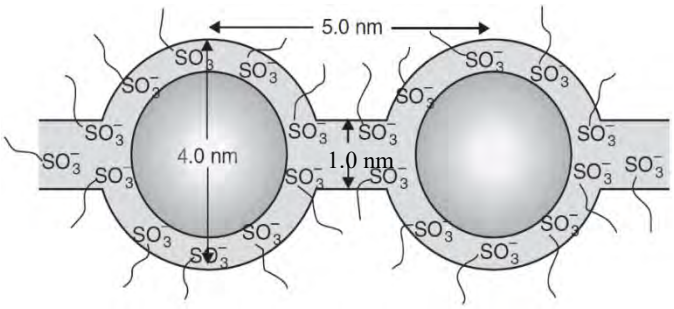

Figure 2.3 Cluster network model for the morphology of hydrated Nafion membranes. (Manthiram et al., 2012)

2.2.2. Electrodes

Electrodes are complex porous structure that through which reactants, reaction products, ions, and electrons. Typically, the electrodes are design as a sequenced of layers as show in Figure 2.4.

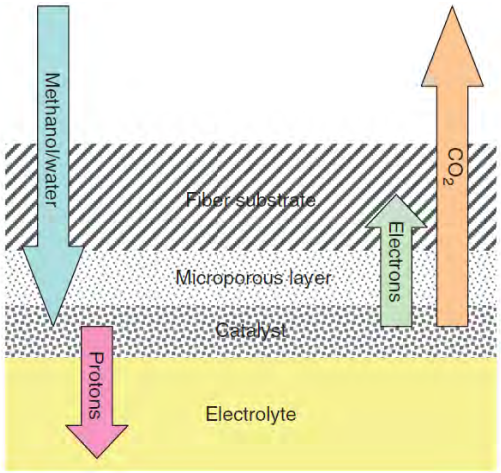

Figure 2.4 Transport effect in DMFC anode. (Jorissen and Gogel, 2009)

- **Catalyst layers**. In this layer, the electrochemical reactions take place, which electrons and protons are generating while methanol and water consumed and carbon dioxide is form as reaction product. Electrons are remove through the adjacent gas diffusion layer and protons are removed via the adjacent electrolyte.

- **Microporous contact layer**. The microporous contact layer (MPL) acts as a current collector as well as a diffusion medium supplying methanol and water as reactant and removing carbon dioxide as product. The MPL typically made from carbon black or graphite powder bound with hydrophobic polymer, such as PTFE.
- **Fiber substrate**. The fiber substrate conducts the electrons that picked up through the MPL to the current collector plates. It is also needs to transport reactants and reaction products. The fiber substrate made from graphitized carbon fibers in the form of a paper or a woven or a nonwoven fabric. In order to allow transport in the gas phase, the fiber substrate is hydrophobized with hydrophobic and electrochemically stable agent.

In a technical electrode, a significant amount of effort needs to be devoted to the handling of reactant supply to and reaction product removal from electrodes (Jorissen and Gogel, 2009).

2.3 Electrochemical Reaction of DMFC System

The reduction and oxidation reaction of DMFC system can take place in acidic and alkaline medium. Oxidation of methanol called methanol oxidation reaction (MOR) and reduction of oxygen called oxygen reduction reaction (ORR). There are some advantages and disadvantages for each medium, it will explain below

2.3.1 Electrochemical Reaction in Acidic Medium

In the acidic medium, the half-cell reaction at anode is

$$CH_3OH + H_2O \rightarrow CO_2 + 6H^+ + 6e^- \quad (2.1)$$

whereas the half-cell reactions at cathode is

$$6H^+ + 6e^- + \frac{3}{2}O_2 \rightarrow 3H_2O \quad (2.2)$$

Therefore, the overall reaction of DMFC in acidic medium is

$$CH_3OH + \frac{3}{2}O_2 \rightarrow CO_2 + 2H_2O \quad (2.3)$$

Equation (2.3) means that methanol reacts with oxygen to produce electric energy with carbon dioxide gas and liquid water as by-product. From equation (2.1) that the oxidation of 1 mol of methanol requires 1 mol of water at the anode. The reduction of oxygen at the cathode generates 3 mol of water, as indicated by equation (2.2). Therefore, an ideal design of the DMFC system should transport part of the water produced at the cathode to the anode compartment (Zhao and Xu, 2009).

At present, DMFCs are mostly using acidic medium. With strong acidic electrolyte membrane, CO_2 generated in anodic reaction can be easy remove. A major contribution to the relatively low DMFC performance is from kinetic constraints in the alcohol oxidation reaction in acid media. (Antolini and Gonzalez, 2010)

2.3.2 Electrochemical Reaction in Alkaline Medium

In the alkaline medium, the mechanism of DMFC shows in Figure 2.5.

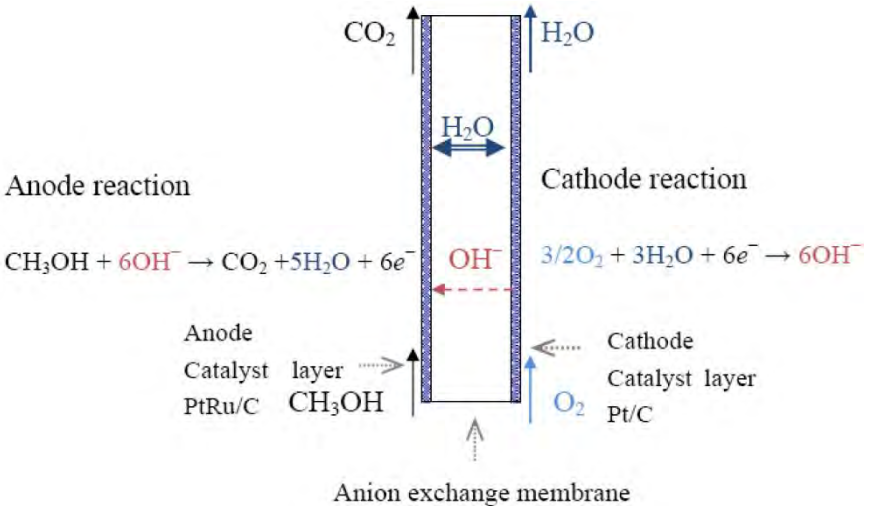

Figure 2.5 Schematic diagram of DMFC in alkaline medium. (Yu et al., 2010)

The reaction and thermodynamics potential (vs. standard hydrogen electrode (SHE)) on each electrode show below

Anode oxidation:

$$CH_3OH + 6OH^- \rightarrow 6e^- + CO_2 + 5H_2O \qquad E^0 = -0.18\ V \qquad (2.4)$$

Cathode reduction:

$$^3/_2\, O_2 + 3H_2O + 6e^- \rightarrow 6OH^- \qquad E^0 = 0.40\ V \qquad (2.5)$$

Overall reaction:

$$CH_3OH + {}^3/_2\, O_2 \rightarrow CO_2 + H_2O \qquad E^0 = 1.21\ V \qquad (2.6)$$

Alkaline medium has numerous advantages over acidic medium. By using basic media, the methanol oxidation kinetics is improving. Another advantage is less corrosive nature of an alkaline environment, therefore large potential use of non-Pt catalysts in the electrodes. The development of new anode and cathode catalyst system is more likely in alkaline media because of the wide range of options for the materials support and catalyst, as compared to acidic media (Antolini and Gonzalez, 2010). Alkaline electrolyte was chosen over acidic medium is to decrease the thermodynamic possibility of corrosion of electrodes (Winterbone and Turan, 2015).

One of problem in alkaline medium is the carbonation of the solution due to CO_2 production

$$2OH^- + CO_2 \rightarrow CO_3^{2-} + H_2O \qquad (2.7)$$

This cause solid precipitations of carbonate salts on the porous electrode and pH decrease in the alkaline electrolyte solution. Consequently, it leads to a reduction in reactivity for fuel oxidation in the system. The application of anion exchange membranes (AEMs) as the solid polymer electrolyte can reduce the formation of carbonate from carbon dioxide, compared to aqueous electrolyte (Yu et al., 2010).

2.4 Anode Electrocatalyst

In DMFC anode, the MOR takes place. The complete electrochemical oxidation of methanol is a multistage process as shown in Figure 2.6 resulting in equation (2.1). The direct pathway represents in principle a dehydrogenation of methanol leading to adsorbed carbon monoxide. In the indirect pathway a reaction cascade started, which leads to different reaction products such as formaldehyde, formic acid and reactive intermediates such as adsorbed HCO and COH. The surface adsorption of these intermediate species can poison the platinum catalyst and thus lead to a low oxidation reaction rate (Zhao and Xu, 2009).

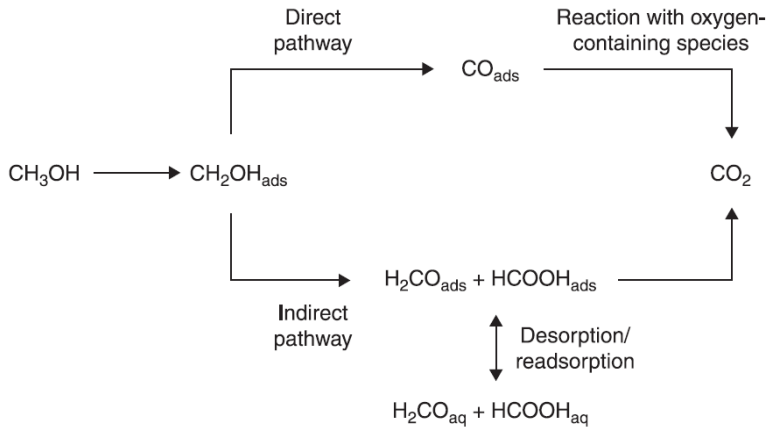

Figure 2.6 Direct and indirect pathway of MOR in electrochemical enviroment. (Hartnig, 2012)

Figure 2.7 shows a comparison of polarization curves for hydrogen and methanol fuel cell. For hydrogen fuel cell, majority of the losses are causes by the oxygen reduction reaction while the polarization caused by the hydrogen oxidation has only a negligible influence. However, in methanol fuel cell case, there is another polarization due MOR in anode. The cell voltage is calculating from the potential difference of the cathodic and anodic polarization curves at a given current density. To overcome the poisoned catalyst and reduce the polarization, we can increase the operating temperature and using more effective catalysts (Jorissen and Gogel, 2009).

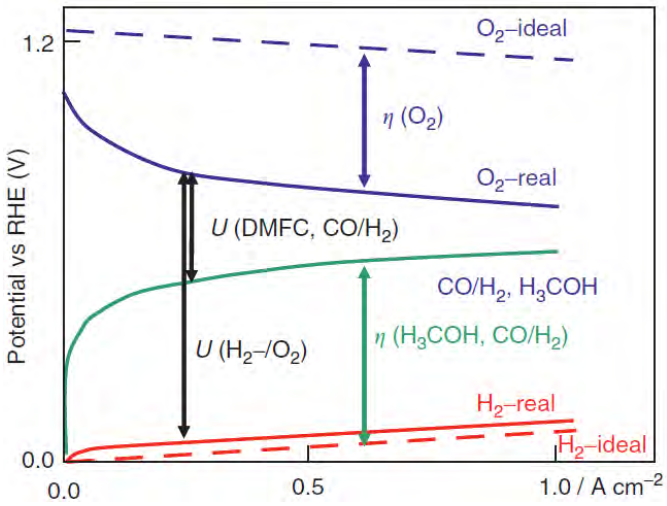

Figure 2.7 Comparison of polarization curve for hydrogen and methanol fuel cell. (Jorissen and Gogel, 2009)

2.4.1 Pt and Pt Based Electrocatalyst

The mechanism of MOR on platinum in alkaline system involves formation of adsorbed methanol species and OH on the Pt surface. The oxidation takes place through a series of reaction step involving successive electron transfer to form adsorbed species. These react with adsorbed OH, to potentially formed carbon dioxide. For other alcohols, the higher energy density and lower toxicity of polyhydric alcohols still attract lots of interest in applying these alcohols in fuel cells, but the electrochemical oxidation is more difficult and the reaction mechanism is more complicated, since it involves breaking C-C bond(s). The reaction at low temperature leads to a low Faradic efficiency (Yu et al., 2010).

To improve the catalytic efficiency and minimize the Pt poisoning by CO, there are many research use bimetallic catalyst, such as Pt-Ru (Xu et al., 2010, Kakati et al., 2011, Liu et al., 2011, Jin et al., 2012, La-Torre-Riveros et al., 2012). The bimetallic catalyst could be a bifunctional catalyst, which platinum is proposed to have the function of adsorbing methanol

$$CH_3OH + Pt \rightarrow Pt - CO + 4H^+ + 4e^- \quad (2.8)$$

and the ruthenium is proposed to have the function of adsorbing water

$$H_2O + Ru \rightarrow Ru - O + 2H^+ + 2e^- \quad (2.9)$$

the metal adsorbates, Pt-CO and Ru-, will react if they are near each other as follows

$$Pt - CO + Ru - O \rightarrow CO_2 + Pt - Ru \quad (2.10)$$

The sum of reactions (2.8) - (2.9) gives the methanol anode reaction (2.1) and regenerates the Pt-Ru catalysts. Although this reaction does initially proceed as written when a bimetallic anode, such as Pt-Ru, is used, unfortunately this reaction eventually slows down to low rates (Gervasio, 2009). Another Pt-based binary alloys, such as PtPd (Chu et al., 2012, Ozturk et al., 2012, Liu et al., 2012, Chu et al., 2013, Wu et al., 2013, Lu et al., 2013, Xia et al., 2014, Zhang et al., 2015a), PtFe (Qiu and Huang, 2012, Xiang and Yin, 2012, Lv et al., 2014b), PtNi (Wang et al., 2013, Nassr et al., 2013, Nassr et al., 2014), PtCo (Qiu and Zou, 2012, Luo et al., 2013, Baglio et al., 2014, Chen et al., 2015b), PtAu (Mikkelsen et al., 2014, Jang et al., 2015, Ren et al., 2015), and ternary alloy, such as PtRuFe (Kim et al., 2012, Wang et al., 2012), PtPdAu (Zhang et al., 2011), PtPdCo (Cho et al., 2014), and quaternary, such as PtRuIrNi (Kim et al., 2013), have been explored also to improve the catalytic activity and overcome the CO poisoning.

Hsieh et al. (Hsieh and Lin, 2009) studied the Pt-M supported carbon nanotube as their catalyst for methanol oxidation. The metal alloys that they used are Fe, Co, and Ni. The study of MOR in H_2SO_4 showed that the bimetallic catalyst has better catalytic activity than the pure Pt/CNT catalyst. Based on cyclic voltammetry (CV) result (Figure 2.8), PtCo/CNT had best catalytic activity towards methanol oxidation. On Pt-Co catalyst, according to the bifuctional mechanism, propose two possible pathways for CO adsorption and OH formation. CO adsorption mainly occurs on Pt, while OH species interact with Co surface. The secondary metal believed to promote electrocatalytic activity and moderate the poisoning of Pt catalyst by supplying OH or other oxygen-containg groups.

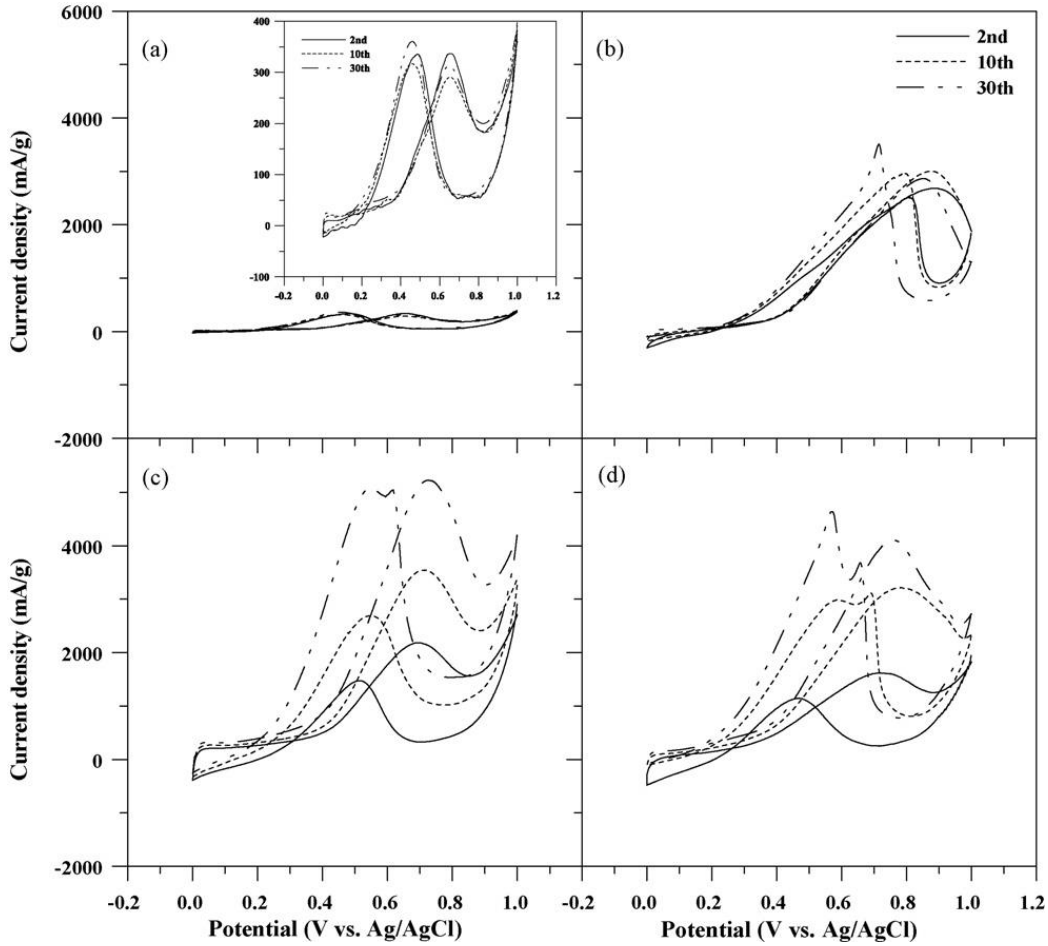

Figure 2.8 Cyclic voltammograms of methanol electrooxidation on different types of Pt and Pt–M/CNT electrodes: (a) Pt, (b) Pt–Fe, (c) Pt–Co, and (d) Pt–Ni. Measurements were performed in 1 M H_2SO_4 + 0.5 M CH_3OH with a scan rate of 10 mVs^{-1} and each arrow in the figures indicates an increase of cycle number. (Hsieh and Lin, 2009)

The second cause of better catalytic activity was due to surface oxides on the sidewalls of CNTs. Similar to the bifunctional effect, the remaining oxide, such as carboxylic and hydroxyl groups will aid in the regeneration of Pt-CO_{ads} sites.

$$CNT - OH + Pt - CO_{ads} \rightarrow CNT + Pt + CO_2 + H^+ + e^- \quad (2.11)$$

The above reaction illustrated the other pathway to strip adsorbed CO from the poisoned Pt sites. Another effect of bimetallic alloy and CNT support was showed in chronoamperometry test to confirm the long-term performance. Figure 2.9 shows the chronoamperometry curves for all catalysts in aqueous electrolyte of 1 M H_2SO_4 + 0.5 M CH_3OH. In the initial stage, all potentiostatic currents found to decrease

rapidly, corresponding to the formation of intermediate species such as CO_{ads}, CH_3OH_{ads}, and CHO_{ads} during methanol oxidation reaction. After 4 h, the current decay becomes gradual and then remains stable. This long time decay attributed to the fact that surface-adsorbed SO_4^{2-} anions on the bimetallic catalysts would restrict methanol oxidation reaction. This proves that bimetallic Pt-Co catalyst seems to be a promising candidate for the DMFCs applications.

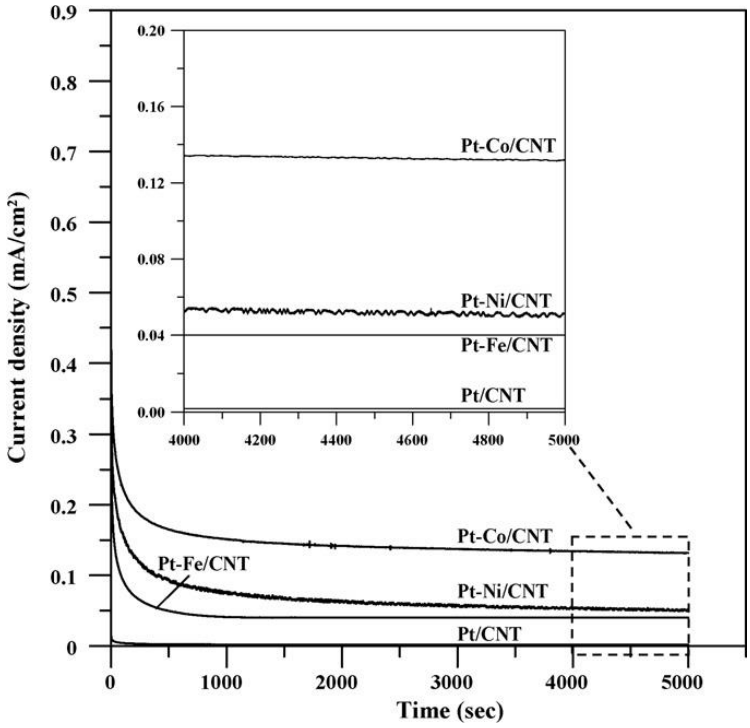

Figure 2.9 Current–time curves for methanol oxidation at 0.45V all electrocatalysts. (Hsieh and Lin, 2009)

2.4.2 Pd and Pd-Based Electrocatalysts

Notable efforts are being carried out to design new catalytic structure for DMFC anodes that not contain Pt and able to oxidize the methanol with reasonable kinetics and tolerable deactivation. Pd considered as an attractive replacement for Pt in DMFC. Pd catalysts are highly active for the oxidation of a large variety substrate in alkaline environment wherein non-noble metals. The dilution of Pd with non-noble metals in a smart catalytic architecture expected to increase the efficiency and decrease the cost of DMFC (Singh et al., 2013).

Ma et al. (Ma et al., 2012) compare the electro-oxidation between Pt/C and Pd/C catalyst in alkaline media. Figure 2.10 (a) and (b) shows the CV curve of the Pt/C and Pd/C catalyst in Ar-saturated 1 M NaOH + ethanol solution at room temperature. It shows the highest current density when 1 M ethanol was used and the Pd/C has higher current density than that on Pt/C. Although the CV profiles of Pt/C and Pd/C are similar, but there are some significant different. The onset potential of ethanol oxidation in Pt/C is shift to higher potential when higher concentration of ethanol is used. However, for Pd/C, the onset potential shows a much smaller shift. This indicate that the ethanol dissociation behavior and the successive intermediates' oxidation behavior on the Pt/C and Pd/C are very different. Presumably, more poisoning species formed on the Pt/C. Figure 2.10 (c) and (d) shows the potentiostatic measurements of the ethanol oxidation on the Pt/C and Pd/C in Ar-saturated 0.1 M NaOH + ethanol solution. It shows that the Faradaic currents on the Pt/C decrease rapidly after applying the potential step. This indicates that more C-C bonds are breaking down on the Pt/C at high potential, which is consistent with the CV measurement results. On the Pd/C electrode, however, the Faradaic current transient behaviors are significantly different from those observed on the Pt/C. The Faradaic currents decrease slowly with the time. This indicates that negligible poisoning species formed on the Pd/C, which is also agreeable with the CV measurement results.

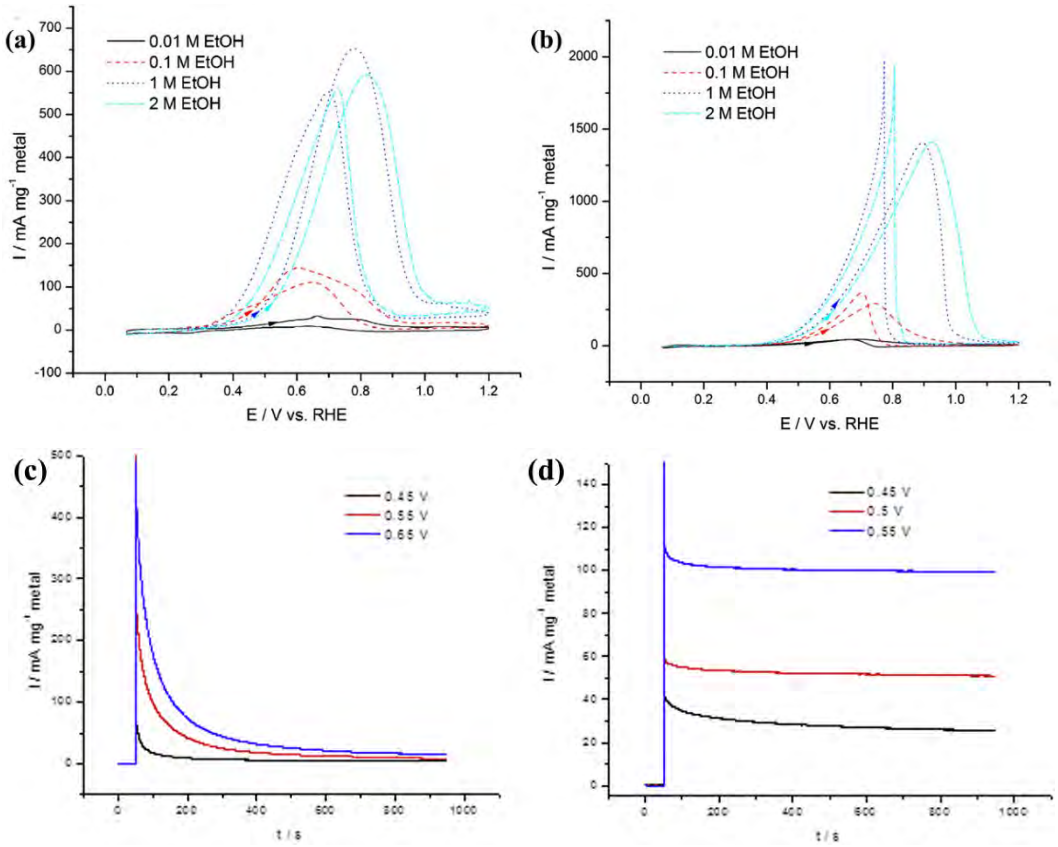

Figure 2.10 The CV curves of (a) Pt/C and (b) Pd/C in 1 M NaOH + ethanol solution, and the CA curves of (c) Pt/C and (d) Pd/C in 1 M NaOH + ethanol solution (Ma et al., 2012)

Due the higher reduction potential of Pd, the size of Pd-base nanoparticles easily controlled down to 10 nm by using weak reduction agents. However, the cost and catalytic activity of monometallic Pd as noble metal still cannot meet the requirements for industrial application. Hence, the construction Pd-based electrocatalyst to replace pure Pd as electrocatalyst has become a significant strategy to improve catalytic performance (Yin et al., 2014). There are some Pd-based bimetallic alloys, such as PdNi (Chen et al., 2015c, Lee et al., 2012, Li et al., 2013, Amin et al., 2014, Choi et al., 2013), PdCo (Wang et al., 2010, Qin et al., 2015), PdFe (Hung et al., 2016), PdAu (Wang et al., 2015, Renjith and Lakshminarayanan, 2015, Maiyalagan et al., 2014), and ternary alloy, such as PdCuSn (Zhu et al., 2015) and CuFePd (Zhang et al., 2015c), which has been explored to improve the catalytic activity of Pd catalyst.

Chen et al. (Chen et al., 2015c) studied about catalytic performances of PdNi/MWCNT for electrooxidation of methanol in alkaline media. Figure 2.11 (a) shows the CV curves in CH_3OH-KOH solution. It shows that the peak current density of PdNi/MWCNT is higher than Pd/MWCNT. The anodic peak of PdNi/MWCNT in the forward scan shift negatively as compared to that of Pd/MWCNT. This phenomenon ascribed to the synergetic effect of nickel. Figure 2.11 (b) shows linear sweep voltammetry (LSV) curves. It shows that the onset potential of PdNi/MWCNT (-0.417 V) was lower than that of Pd/MWCNT (-0.368 V). These results indicated that the addition of nickel into the Pd-based catalyst effectively decreased the overpotential of methanol oxidation. Figure 2.11 (c) shows the chronoamperometry (CA) for evaluate the poison resistance of catalysts. In methanol oxidation, the performances loss ratios of Pd/MWCNT and PdNi/MWCNT are 81.4% and 75.3, respectively. This result indicates that the addition of nickel into the Pd-based catalyst improves the poison resistance of Pd/MWCNT, considering the existence of nickel hydroxides.

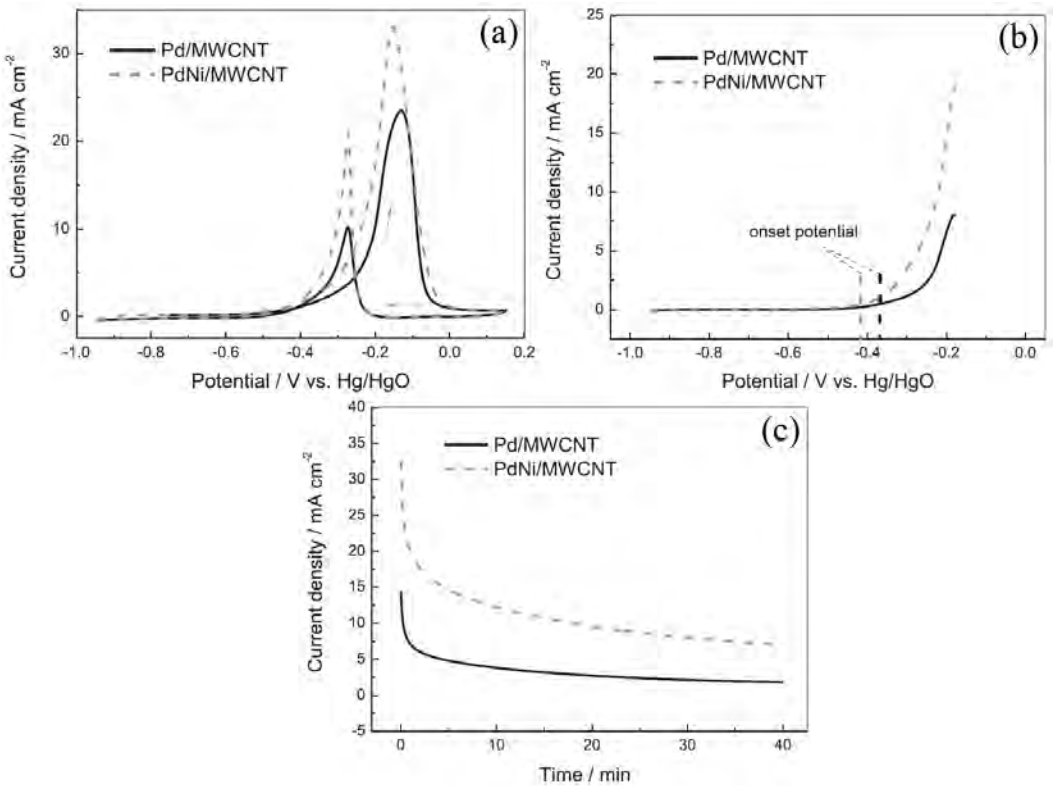

Figure 2.11 (a) CV curves, (b) LSV curves, and CA curves of catalyst recorded in 1 M CH_3OH + 1 M KOH solution. (Chen et al., 2015c)

2.5 Electrocatalysts Preparation Method

Several methods had been reported for the preparation of DMFC electrocatalyst, some of them are describe below:

2.5.1 Impregnation Method

In the impregnation method, the support is impregnate by suitable metal precursor solution. The dispersed metal ions are reduced by using reducing agents, such as $NaBH_4$ (Zhang et al., 2015c, Zhu et al., 2015, Lv et al., 2014a) and ethylene glycol (EG) (Chen et al., 2015b, Chen et al., 2015a, Li et al., 2014, Nassr et al., 2013). Generally, metal chloride salts, such as $PdCl_2$, $NiCl_2$, $CoCl_2$, and $FeCl_3$, are use as metal precursors.

2.5.2 Sol-Gel Method

Nasser et al. (Barakat et al., 2013) had prepared cadmium-doped cobalt/carbon as nonprecious electrocatalyst for methanol oxidation. They were used cobalt (II) acetate tetra-hydrate and cadmium acetate dihydrate as the precursors. They mixed them in the poly(vinyl alcohol) as their solvent and did thermal treatment at controlled atmosphere. Salazar-Banda et al. (Salazar-Banda et al., 2012) prepared their Pt-based ternary and quaternary electrocatalyst in for methanol oxidation also by using sol-gel method.

2.5.3 Hydrothermal Method

By using hydrothermal method, some catalyst had synthesized. Kakati et al. (Kakati et al., 2012) prepared Pd@Mo (at pH~2 and pH~7) and Mo@Pd (at pH~5 and pH~9) nanoparticles deposit on (multi-walled carbon nanotubes) MWCNT by using $PdCl_2$ and $MoCl_2$ as the metal source and EG as reducing agent under hydrothermal condition. The hydrothermal process was taken at 160 ^oC for 5 h. Liu et al. (Liu et al., 2015) also prepared their Pd nanoparticles supported on three-dimensional graphene aerogels by using hydrothermal method. They mixed $PdCl_2$, $NaBH_4$ and graphite oxide suspension in teflon-lined autoclave. The hydrothermal condition was at 180 ^oC for 12 h.

2.5.4 Electrodeposition Method

Zhao et al. (Zhao et al., 2014) prepared their catalysts, Pt-Ru and Pt-Ru-Ni nanocluster on MWCNT by using electrodeposition method. The deposition of Pt and Ru was take place in K_2SO_4 solution with K_2PtCl_6 and $RuCl_3$ as metal precursor by using the potential step method. The potential was jump from 0.3 V to 1.1 V with pulse width 0.001 s and this was repeat until a steady pulse current was reach. The surface complex of MWCNT that had been modify, were converted into PtRu nanoparticle clusters through cycling from +1.0 to - 0.26 V in 0.1 M H_2SO_4 solutions to the steady state. Su et al. (Su et al., 2015) prepared their bimetallic Pt_3Co nanowires (NWs) by using electrodeposition method. The electrodeposition experiment carried out by using three-electrode potentiostatic control with a

saturated calomel electrode (SCE) as the reference electrode and the Ag-coated anodic aluminum oxide (AAO) template as the working electrode. They were adjusted the Co^{2+} concentration in electrolyte higher than Pt^{4+}, due to extremely high rodex potential of Pt^{4+} than that of Co^{2+}. Following the electrodeposition, the Pt_3Co NW array were annealed for 2h in H_2 (5%)/N_2 (95%).

2.5.5 Emulsion Method

The emulsion method is a novel route for the formation of nanoparticles (NPs). An emulsion is a cloudy colloidal system of micron size droplets of one immiscible liquid dispersed in another, such as oil in water, in the presence of a suitable surfactant and a co-surfactant. An emulsion is form by vigorous stirring or sonication and is thermodynamically stable. Nano size particles can spontaneously form within the micron size water droplets as a thermodynamically stable emulsion. Briefly, in this method the first step is the formation of NP through a water-in-oil emulsion reaction, followed by a reduction step. The surfactant molecules can function as protective agents to prevent the NP from agglomeration. The surfactant molecule can be easily remove by heat treatment. The main advantage of the emulsion method is its controlling metallic composition and particle size with a narrow distribution (Singh et al., 2013).

Lee et al. (Lee et al., 2012) prepared 5 nm Pd-Ni nanoalloys for electrocatalyst ethanol oxidation. They dissolved palladium (II) acetylacetonate ($Pd(acac)_2$) and nickel (II) acetylacetonate ($Ni(acac)_2$) as metal precursors, and tetra-butylamine-borane (TBAB) as reducing agent in a mixture of oleic acid (OAc) and oleylamine (OAm). The mixture first stirred at room temperature for 30 min under an argon flow, then the solution heated to 270 ºC for 20 min. The resultant solution was cooled down to room temperature, the final product was washed and separated by centrifugation. For preparation of PdNi/C catalyst, the PdNi nanoparticles and Ketjen black carbon were mix with hexane and sonication. After the hexane is evaporate, acetic acid was poured into the catalyst and vigorously stirred at 80 ºC overnight. The final product was wash with ethanol and separated by centrifugation. The transmission electron microscopy (TEM) results, shown in

Figure 2.12, shows the Pd-Ni alloy NPs formed homogeneous NPs and chemically dealloyed with the carbon support. Acid treatment was chosen for eliminate residual organic surfactant. Interestingly, from inductively coupled plasma-atomic emission spectroscopy (ICP-AES) analysis, the $Pd_{50}Ni_{50}$/C was change to $Pd_{86}Ni_{14}$/C. This ascribed to the selective dissolution of the Ni component from the Pd-Ni alloy NPs during the acid treatment.

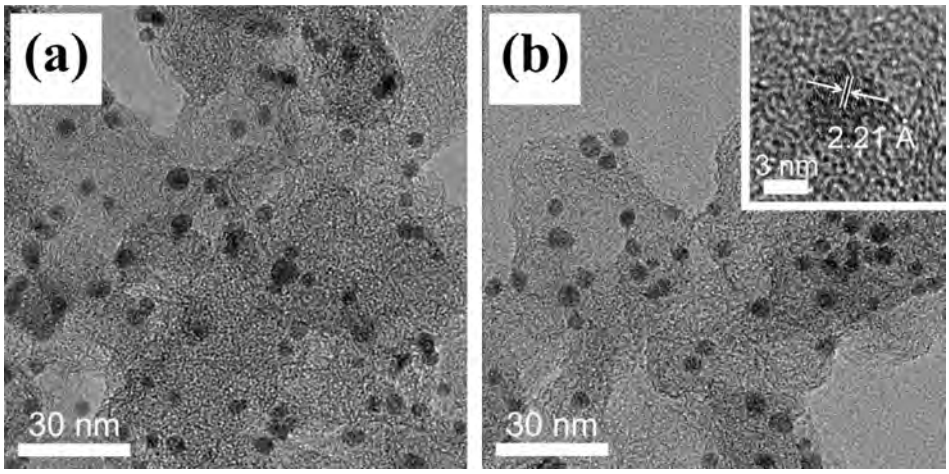

Figure 2.12 (a) TEM images of carbon supported $Pd_{50}Ni_{50}$ NPs and (b) TEM and HRTEM images of $Pd_{86}Ni_{14}$/C. (Lee et al., 2012)

Choi et al (Choi et al., 2013) prepared 9 nm Pt-Ni for oxygen reduction reaction. In a typical synthesis, $Pt(acac)_2$ and $Ni(acac)_2$ were mixed with OAm and OAc in benzyl ether, followed by the addition of $W(CO)_6$ at 130 °C under Ar protection. The mixture then heated to 230 °C, while the Ar purging stopped at the same time. To control the Pt/Ni ratio, they treated the Pd-Ni with acetic acid (HAc) at 60 ºC. The 9 nm Pt−Ni octahedra were obtained after the reaction was allowed to proceed at 230 °C for 40 min. Figure 2.13 (a) shows a TEM images of carbon supported Pd-Ni octahedra. The Pd-Ni catalysts have an average edge length of 9 nm and good size uniformity. The high-resolution TEM (HRTEM) shows the d-spacing for adjacent lattice fringes was 2.25 Å (±0.05), which smaller than that (2.27 Å) of planes of face-centered cubic (FCC) bulk Pt.

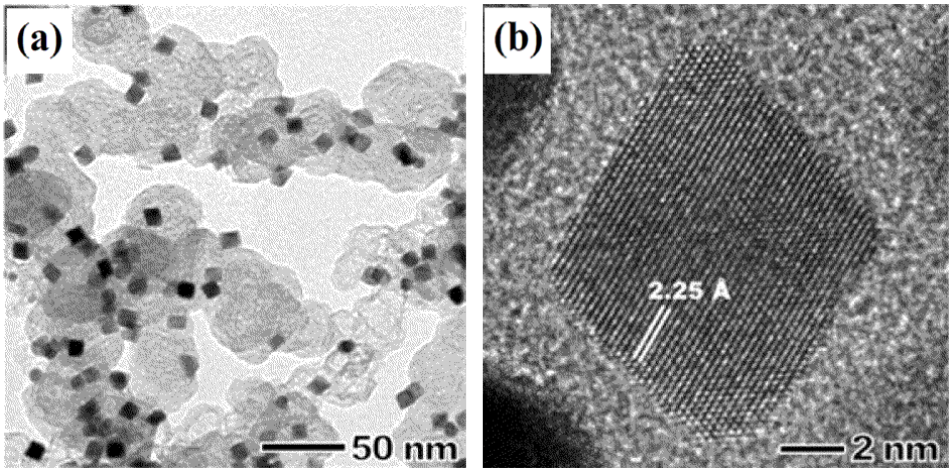

Figure 2.13 (a) TEM and (b) HRTEM images of carbon supported Pt-Ni catalyst

2.6 Ternary Alloy Catalyst for Methanol Oxidation

Developing solid solutions with a second or third metal is a convenient way to achieve dual aims of increasing their activity and reducing their noble metal content in order to overcome the poisoning effects by reducing surface coverage by adsorbed CO (Arikan et al., 2013). The ternary alloy has activity, stability, CO poisoning tolerance and durability are superior to their binary counterparts due to the alteration of electronic and adsorption properties (Zhang et al., 2015b).

Zhang et al. (Zhang et al., 2015c) studied about CuFePd supported reduced graphene oxide (rGO) on electrocatalytical activity for the methanol oxidation reaction. They synthesized their catalyst by using impregnation method with $NaBH_4$ as a reducing agent. They compared the physical and electrochemical properties of the catalysts. The XPS results of CuFePd/rGO (Figure 2.14) show the peaks of C 1s, Pd 3d, Cu 2p, and Fe 2p. The CuFePd/rGO were successfully fabricated which indicated by XPS spectra of Pd $3d_{5/2}$ and $3d_{3/2}$, Cu $2p_{1/2}$ and $2p_{3/2}$, and Fe $2p_{1/2}$ and $2p_{3/2}$.

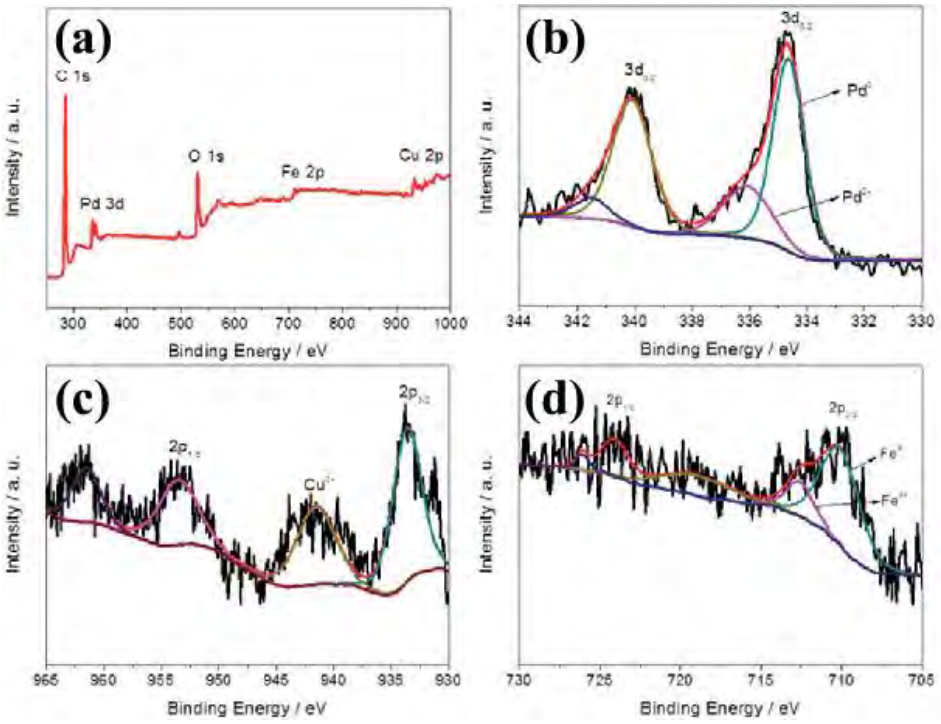

Figure 2.14 XPS spectra of (a) CuFePd/rGO, (b) Pd 3d, (c) Cu 2p, (d) Fe 2p. (Zhang et al., 2015c)

The electrocatalytic performance of the catalysts in 1 M NaOH + 1 M CH_3OH solution also observed. The CuFePd/rGO have better catalytic activity for MOR than that on the CuPd/rGO, FePd/rGO, and Pd/rGO. It show on Figure 2.15 (a), the current density of CuFePd/rGO is higher than that on the Pd-based binary alloy and mono-Pd supported rGO. This indicated that the present of Cu and Fe reduce the coverage of CO-like carbonaceous species on the Pd surface was reduce, making more active sites available for MOR (Scofield et al., 2015). The stability test of the catalysts was observe by CA method, as shown in Figure 2.15 (b). The ternary CuFePd/rGO catalyst maintained the highest steady state current density than that on binary FePd/rGO and CuPd/rGO as well as the monometallic Pd/rGO. This suggest that the ternary CuFePd/rGO catalyst has enhanced stability for MOR.

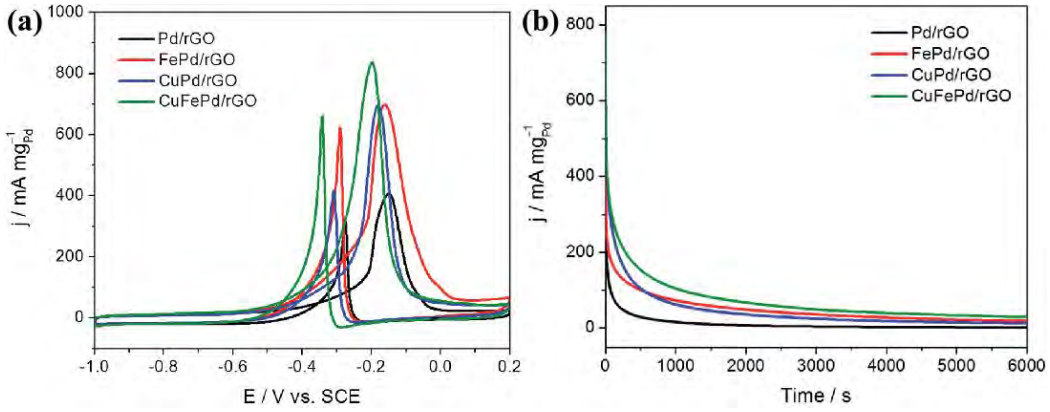

Figure 2.15 (a) CV curves Pd/rGO, CuPd/rGO, FePd/rGO, CuFePd/rGO, and (b) CA curves of Pd/rGO, CuPd/rGO, FePd/rGO, CuFePd/rGO. (Zhang et al., 2015c)

2.7 Carbon Support

The purpose of nanoscaling of the catalyst is to form more active sites per mass unit. In this case, nanosized metallic catalyst particles must be loaded on certain support preventing them from aggregation and/or sintering during the synthesis and fuel cell operation. There are some kind of carbon support that have been used as support materials in catalyst, such as carbon black, activated carbon, graphite, and graphitized materials. Carbon black is most commonly use as support in catalyst.

CHAPTER III
EXPERIMENTAL DETAIL

3.1 Materials

$Pd(acac)_2$, $Ni(acac)_2$, $Co(acac)_2$, and $Fe(acac)_3$, which purchased from New Jersey, were used as metal precursors. Benzyl alcohol was used as a reduction agent in the present of oleic acid as a stabilizer and oleylamine as co-reductant and co-surfactant. Toluene and ethanol were used in washing process of solution and surfactant. XC72R is a type of carbon black powder was used as a carbon support. Distilled water was used throughout this study. The used materials were listed in

Table 3.1 Materials selection for experimental

Chemical Name	Formula	Purity	Phase	Manufacturer
Palladium (II) acetylacetonate	$C_{10}H_{14}O_4Pd$	35%	Solid	Fisher Scientific Acros
Nickel (II) acetylacetonate	$C_{10}H_{14}NiO_4$	96%	Solid	Fisher Scientific Acros
Cobalt (II) acetylacetonate	$C_{10}H_{14}CoO_4$	99%	Solid	Fisher Scientific Acros
Iron (III) acetylacetonate	$C_{15}H_{21}FeO_6$	99+%	Solid	Fisher Scientific Acros
Benzyl alcohol	C_7H_8O	99%	Liquid	Fisher Scientific Acros
Oleylamine	$C_{18}H_{37}N$	80-90%	Liquid	Fisher Scientific Acros
Oleic acid	$C_{18}H_{34}O_2$	90%	Liquid	Sigma Aldrich
Toluene	$C_6H_5CH_3$	99.8+%	Liquid	Fisher Scientific Acros

3.2 Experimental Procedures

3.2.1 Synthesize Pd/C catalyst

Pd/C catalyst was prepared by reduction method. The synthesize of 40 wt% Pd/C started by mixing 50 mg XC72R carbon black and 55.54 mg $PdCl_2$ in a solution containing 50 mL 1 M monosodium citrate ($C_6H_7NaO_7$) and 100 mL ethanol. The mixture was ultrasonicated to dispersing the powder. Then the mixture was stirred and heated at 80 °C for 30 min. The powder was collected by filtering and washing with DI water. The final product was collected after freeze drying the suspension overnight.

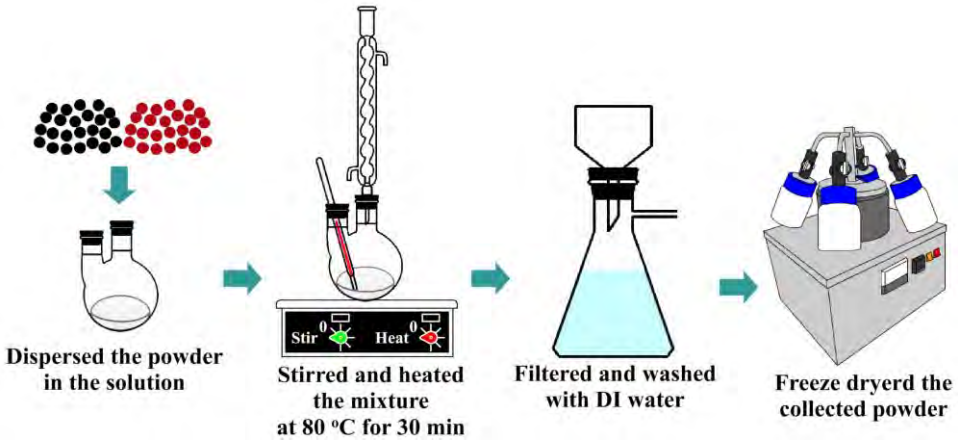

Figure 3.1 Schematic of synthesize of Pd/C

3.2.2 Synthesize of Pd-based Ternary Alloys

Pd-based catalysts were prepared by emulsion method. The synthesize started by dispersing $Pd(acac)_2$ and the other metal precursors in the solution containing benzyl alcohol (BA), oleylamine (OAm) and oleic acid (OAc). To study the effect of different metal alloy in ternary alloy catalyst, PdNiCo, PdFeCo, and PdNiFe ternary alloy were prepared with the initial molar ratio 3:1:1. To study the effect of reducing agent volume, volume ratio 0.5, 0.7, and 0.9 of reducing agent to total volume were prepared and the ratio between oleylamine and oleic acid were fixed 1:2. The mixture was purged with nitrogen gas then heated for 30 minutes for reduce the metal precursors. To study the effect of reduction temperature, 110, 130, 150 °C were used. Then the mixture continues heated for started the alloying to

200 ºC and held it for 40 minutes. After cooling down, the mixture was put in centrifuge tube for washing with toluene one time and ethanol three times. The collected powder was got after dried the suspension in freeze dryer overnight. Figure 3.2 shows the experimental process.

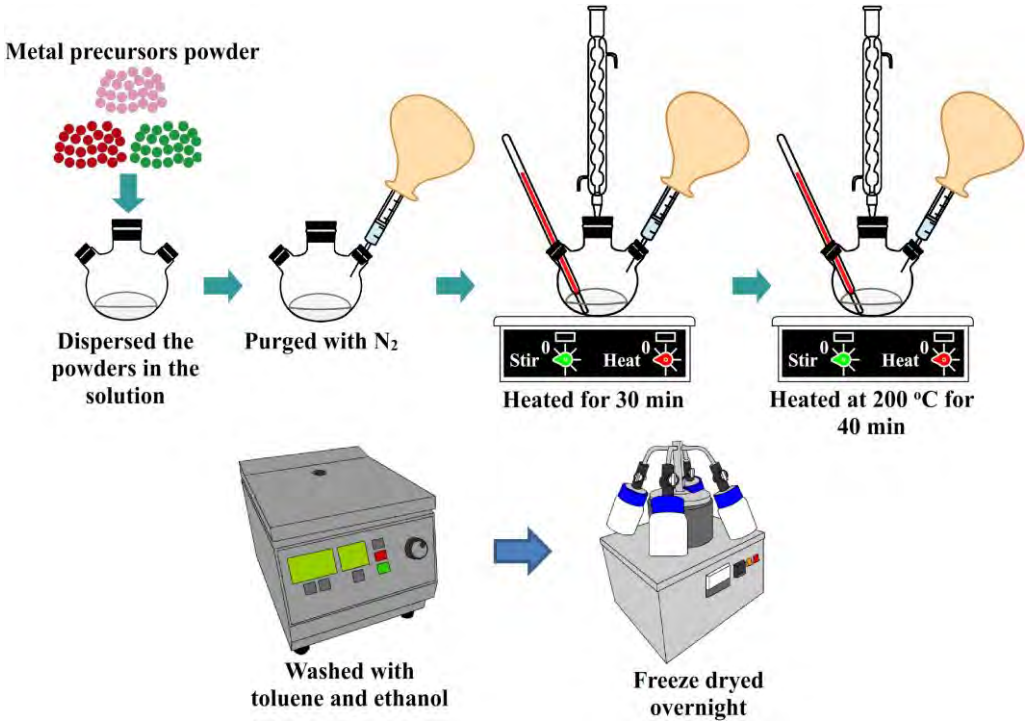

Figure 3.2 Schematic of synthesize of Pd-based ternary alloy

3.2.3 Synthesize Pd-Based Ternary Alloy Supported XC72R

The 40 wt% Pd-based catalyst supported XC72R prepared by using rotary evaporated method. First the Pd-based ternary alloy was mixed with XC72R in 10 mL ethanol. The mixture was sonicated for 20 min to dispersing the powder. Then the mixture was put into the rotary evaporator machine. The vacuum pressure was 90 hPa and the evaporation temperature was 40 ºC. The catalyst powder was collected after the solution evaporated. Figure 3.3 shows schematic of rotary evaporation method.

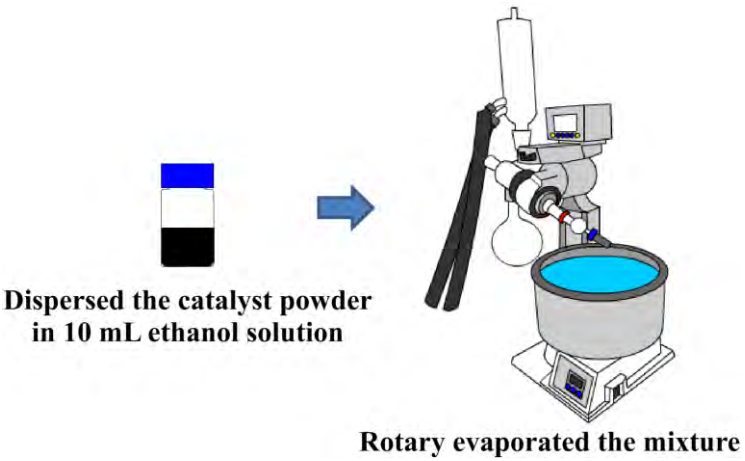

Figure 3.3 Schematic rotary evaporator method

3.3 Flowchart of Experimental

The experimental procedure for synthesize 40 wt% Pd/C was explained by the flowchart which shown in Figure 3.4.

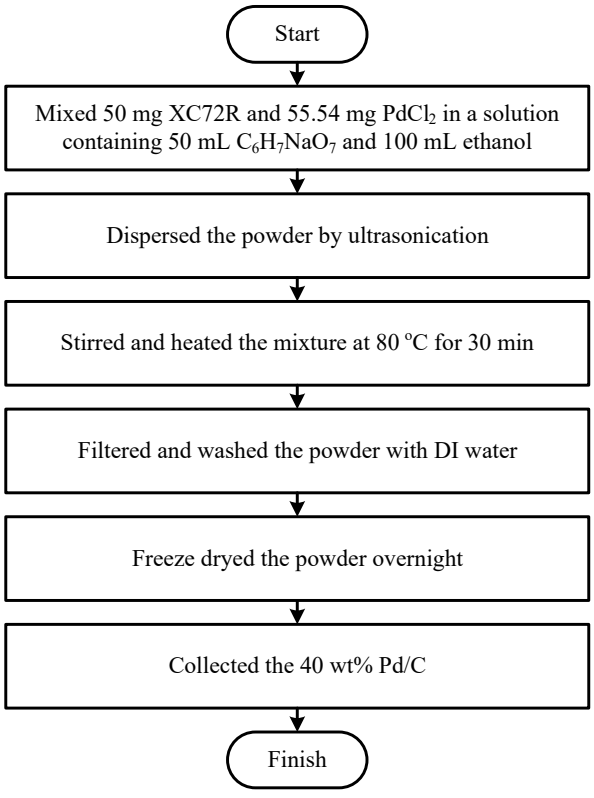

Figure 3.4 Flowchart of synthesize Pd/C

The experimental procedures for synthesize 40 wt% Pd-based ternary alloy supported XC72R were described in Figure 3.5.

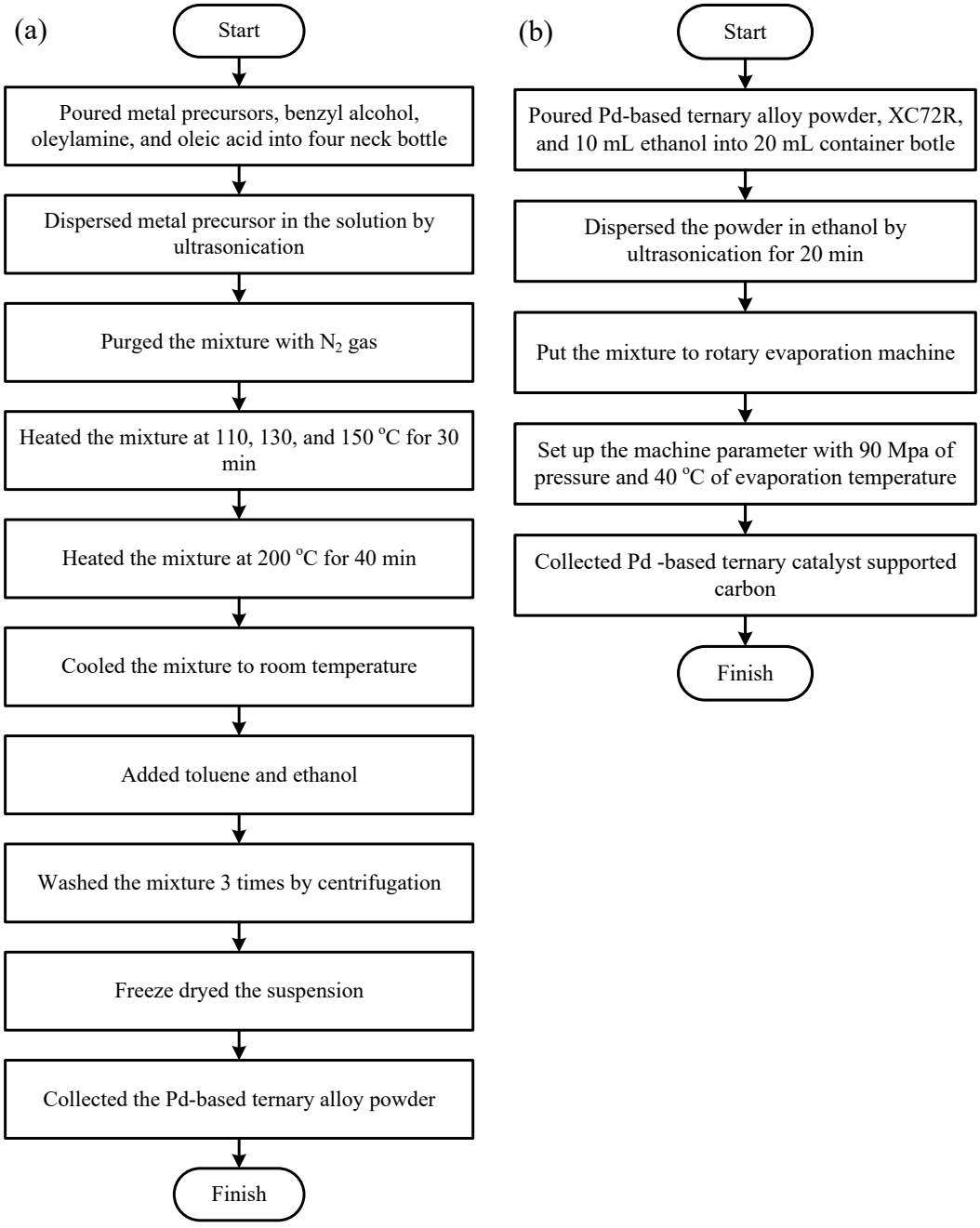

Figure 3.5 Flowchart (a) synthesize Pd-base ternary alloy and (b) Pd-based ternary alloy supported carbon black

3.4 Experimental Matrix

In this research, there are some variables have been studied including molarity of reductant, reduction temperature, and different alloying element.

Table 3.2 Parameter control for experimental

Variable	Ternary Alloy Catalyst	Metal Precursors	Volume ratio of Reducing Agent to Total Volume	Reduction Temperature (°C)
Reductant molarity	PdNiCo/C	$Pd(acac)_2$, $Ni(acac)_2$ $Co(acac)_2$	0.5	130
			0.7	
			0.9	
Reduction Temperature	PdNiCo/C	$Pd(acac)_2$, $Ni(acac)_2$ $Co(acac)_2$	0.7	110
				130
				150
Metal Precursors	PdNiCo/C	$Pd(acac)_2$, $Ni(acac)_2$ $Co(acac)_2$	0.9	150
	PdFeCo/C	$Pd(acac)_2$, $Fe(acac)_3$ $Co(acac)_2$		
	PdNiFe/C	$Pd(acac)_2$, $Ni(acac)_2$ $Fe(acac)_3$		

3.5 Materials Characterization

3.5.1 X-Ray Diffraction

X- Ray Diffraction (XRD) is structural analysis to determine the orientation of a crystal or grain, determine the crystal structure of material, and the average spacing of atoms. X rays are produced when high speed electrons collide with target.

A hot tungsten filament has high accelerating voltage between cathode and anode. Some parameter was decided for measurement including of increment angle, 2θ range, scanning time, and rotation degree. For this study, all of samples are measured in an angle range 2m0-90° using X-Ray Diffraction: Bruker D2 Phaser. Figure 3.6 Bruker D2 Phaser XRD shows the instrument image. The spectra use Cu Kα (λ = 1.5406 Å), Ni filter, 40 kV, and 100 mA. Low scanning rate was set with step size of 0.0081° and time of 0.1 second per step.

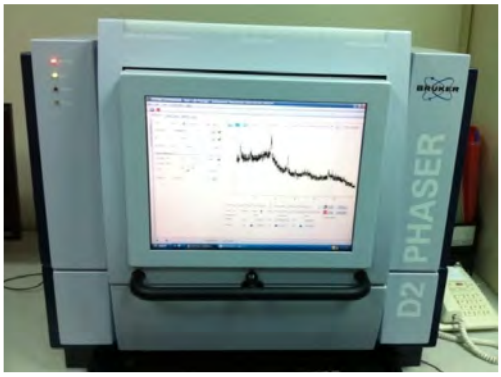

Figure 3.6 Bruker D2 Phaser XRD

The grain size of particle, τ, is estimate from the half-height width of the diffraction peak (111) using the Scherrer formula:

$$\tau = \frac{(k\lambda)}{(\beta \cos \theta)} \tag{3.1}$$

where τ is the grain size (in nanometers), λ is the wavelength (in nanometers), β is the full width at half-maximum FWHM) (in radians), k is a constant (0.94 to spherical crystallites) and θ is the diffraction angle.

An estimative of lattice parameter calculated from equation (3.2):

$$n\lambda = 2d_{hkl} \sin \theta \tag{3.2}$$

where n represents the reflection order, λ is the wavelength (in nanometers), d_{hkl} is interplanar distance between two planes with Miller indices hkl, and θ is the incident angle of X-rays.

3.5.2 Scanning Electron Microscopy

Scanning Electron Microscopy (SEM) was carried out to see the morphology of powder catalyst. For preparation step, powder samples coated by platinum for 60 seconds to avoid charge effect and then observed the image using SEM JEOL JSM 5800 with 10 kV. Figure 3.7 SEM-JEOL-JSM-5800

Figure 3.7 SEM-JEOL-JSM-5800

3.5.3 Transmission Electron Microscopy

Scanning Electron Microscopy (SEM) was carried out to see the morphology of powder catalyst in high resolution and the selected area electron diffraction (SAED). For preparation step, the Pd-based ternary alloy was dispersed in a polymer solution to form a bulk sample after heat treatment. The samples cut with laser beam, and put on Cu grips. Figure 3.8 shows the TEM machine.

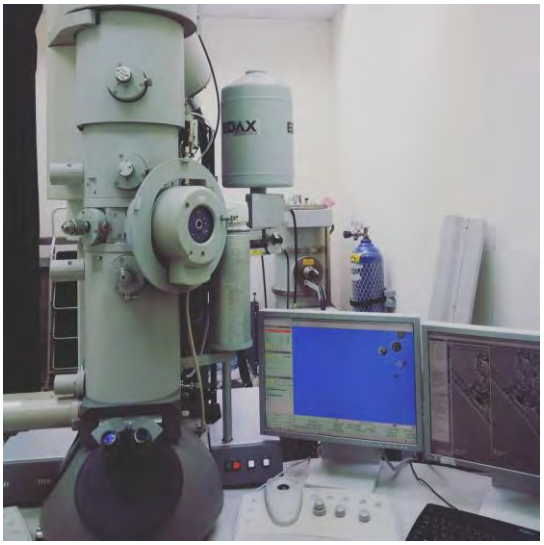

Figure 3.8 Tecnai F20 G2 FEI-TEM

3.6 Electrochemical Characterization

Identification of MOR performance was done by using VSP-Biologic Science Instrument (Figure 3.9 VSP-Biologic Science Instrument. The working electrode was prepared with a catalyst ink-coated glassy carbon (GC) disk. The metal loading of catalyst was 28 μg cm^{-2}. The catalyst ink was prepared by mixing 16.63 mg catalyst powder with a solution containing 6 mL propanol and 14 mL DI water. The working electrode was prepared by dropping 20 μL catalyst ink and dry surface was covered by 5 μL 0.1 wt% nafion. The cyclic voltammetry (CV) measurement was performed using conventional three electrodes electrochemical cell. The counter and reference electrode were Pt wire and reversible hydrogen electrode (RHE), respectively. The electrochemical active surface area (ESCA) was got from CV measurement in 1 M KOH solution. The ESCA was calculated from PdO reduction region with PdO charge was 0.434 mC cm^{-2}. The MOR performance was carried out in a solution containing 1 M KOH and 1 M CH_3OH. The CV was run with scan rate 50 mV s^{-1} and conducted in nitrogen saturated from 0.1 to 1.2 V. The chronoamperometry (CA) was done to studying the stability of catalyst. The CA was conducted in a solution containing 1 M KOH and 1 M CH_3OH with initial potential 0.7 V for 1 h.

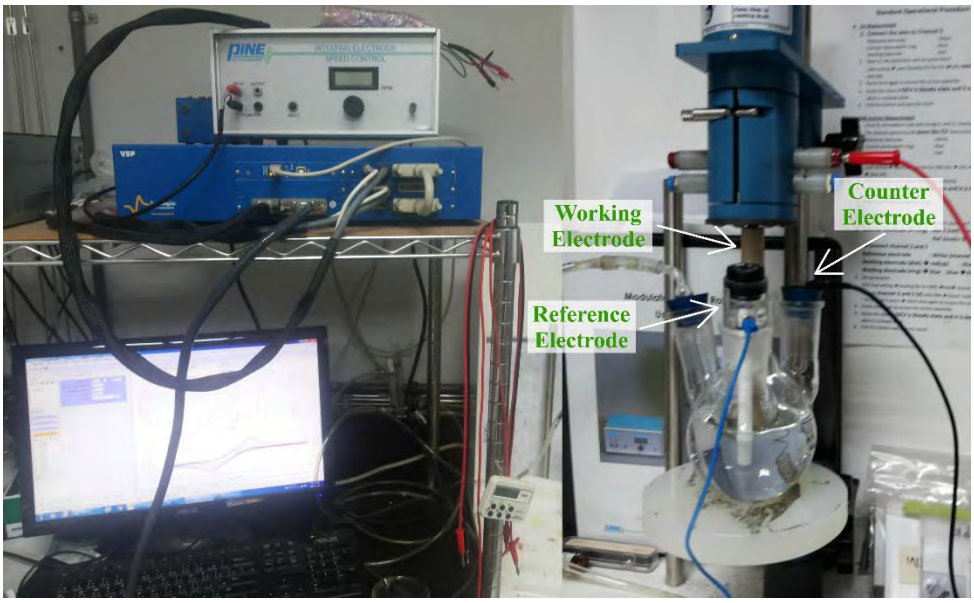

Figure 3.9 VSP-Biologic Science Instrument

CHAPTER IV
RESULTS AND DISCUSSIONS

4.1. Characterization of Pd/C catalyst

Pd/C catalyst was synthesized by commonly reduction method which using $C_6H_7NaO_7$ for reduce the $PdCl_2$ nanoparticles. The XRD pattern shows in Figure 4.1. The first peak located at around 25º in XRD pattern is attributable to the Vulcan XC-72 carbon black as support material. The other peaks are the characteristic of face centered cubic (FCC) crystalline Pd at 2θ values of 40.24º, 46.66 º, 68.12º, and 82.10º and indexes with planes (111), (200), (220), and (311), respectively. The calculated d-spacing (Vegard, 1921) from (111) peak is 0.221 nm. These results confirm by JCPDS 46-1043 of Pd, indicates the formation of pure Pd NPS. The grain size of 7.7 nm obtains from the width of the peak (111) by the Debye-Scherrer's formula (Vegard, 1921).

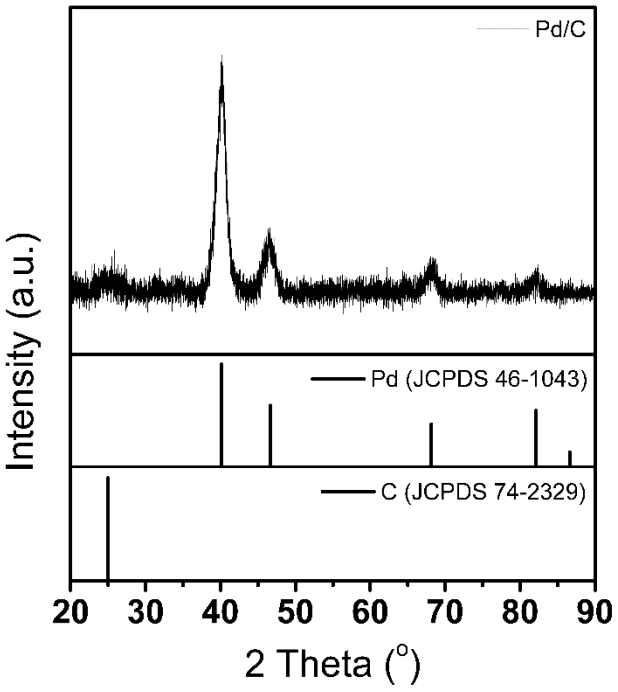

Figure 4.1 XRD pattern of Pd/C

Figure 4.2 shows SEM images of Pd/C. The secondary electron (SE) image shows particle formed a rounded structure and some of them aggregated. The backscatter electron (BSE) mode of SEM conducted to know the existence and shape of catalyst. The BSE image shows the catalyst particles because it has larger electron number. The BSE images shows the existence of catalyst particles in spherical and aggregate shape. The aggregate structure is due to the attractive van der Waals potential of each particle (Wang and Tseng, 2009).

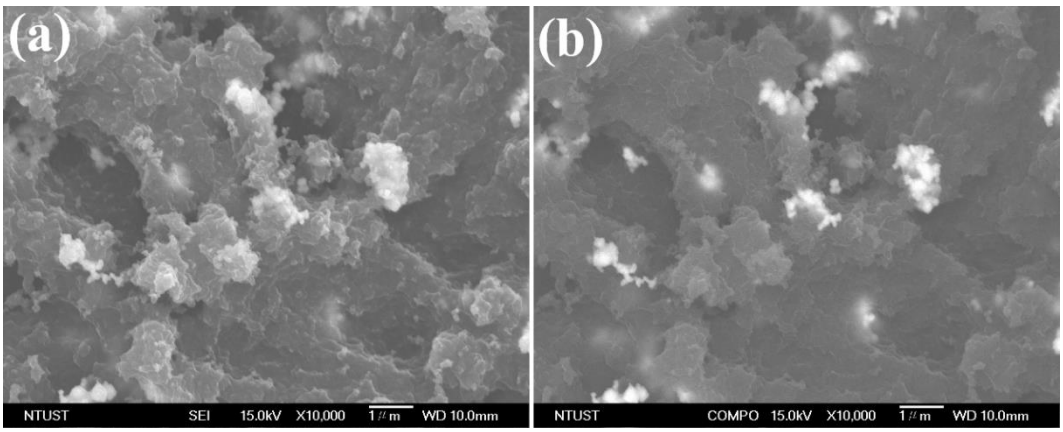

Figure 4.2 (a) Secondary electron and (b) backscattered electron mode of SEM images of Pd/C

Figure 4.3 shows the TEM images of the as-prepared Pd/C. The low-resolution TEM image (Figure 4.3(a)) shows the spherical nanoparticle with the average particle diameter of 7.0 nm, which confirms the XRD result above. The nanoparticles are successfully attach on the XC-72. The SAED image in Figure 4.3 (b) confirms the XRD pattern that the Pd/C are polycrystalline structure, with crystallography orientation in (111), (200), (220), and (311) direction. The interplanar spacing of 0.226 nm observed at most region on Pd/C surface, close to the (111) lattice spacing of FCC Pd (0.224 nm).

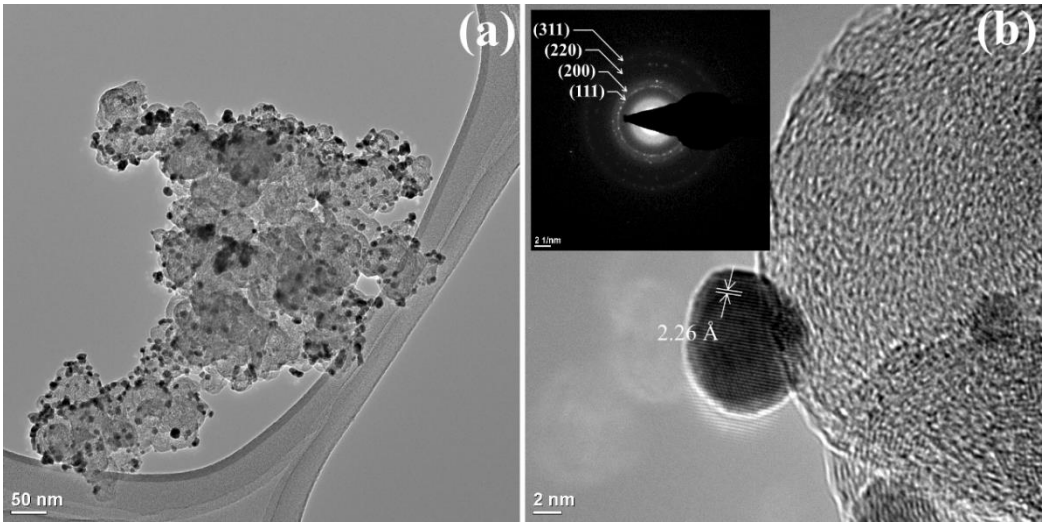

Figure 4.3 (a) Low resolution TEM and (b) magnified TEM with inset shows SAED image of Pd/C

The electrochemical activity of catalyst observed from the CV measurement. Figure 4.4 (a) shows the measured CV pattern of Pd/C in 1 M KOH solution. Small peak at 0.46 V ascribed to adsorption of OH^- on the surface of catalyst (Wang et al., 2014). A broad peak at 0.73 V can ascribed to the reduction of the Palladium (II) oxide during negative scan (Ren et al., 2014). From this region, the ESCA can calculate which has value of .0.446 cm^2. The methanol activity of Pd/C catalyst measured in a methanol solution containing 1 M KOH + 1 M methanol. The Figure 4.4 (b) shows the CV curve of Pd/C in methanol solution. The peak at forward scan assigned to the oxidation of freshly chemisorbed species coming from the adsorption of methanol; the backward oxidation peak is primarily associated with the removal of carbonaceous species that not completely oxidize during the forward scan (Mancharan and Goodenough, 1992). In general, the magnitude of the peak current in the forward scan indicates the electrocatalytic activity of the electrocatalysts for methanol oxidation (Wang et al., 2014).

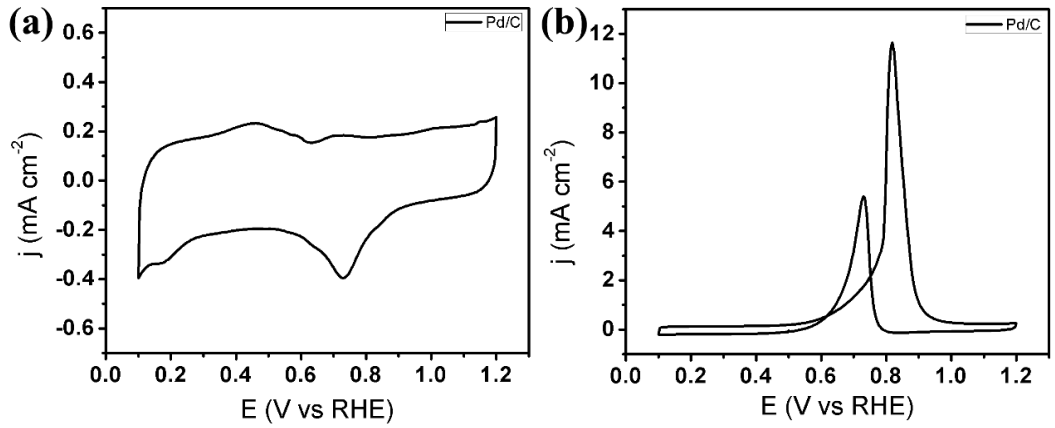

Figure 4.4 CV result of Pd/C catalyst in (a) 1 M KOH and (b) 1 M KOH + 1 M methanol solution

4.2. Effect of Synthesis Parameters on Physical Properties and Catalytic Activity of Electrocatalysts

The synthesis parameter of emulsion method will be affected the physical properties of catalyst. Fang and co-workers (Zhang et al., 2010) purposed the emulsion method for synthesized the catalyst. Mostly the parameter can be controlled are volume of reducing agent in solution and reduction temperature. This study conducted to finding best parameter for synthesis the nanoparticle of catalysts.

4.2.1. Effect of Volume Ratio on Properties of Catalyst

Volume ratio of reducing agent to total volume will be affected the physical properties of nanoparticles. As shown in Figure 4.5 (a), there are peaks of Pd (111), (200), (220), and (311) in XRD pattern of PdNiCo/C. With addition of transition metal, the diffraction peaks of ternary alloy catalyst shift to higher 2θ values. As shown in Figure 4.5 (b), the 2θ of Pd (111) peak is slight shift to higher angle. The same trend replicated for Pd (200), Pd (220), and Pd (311) diffraction.

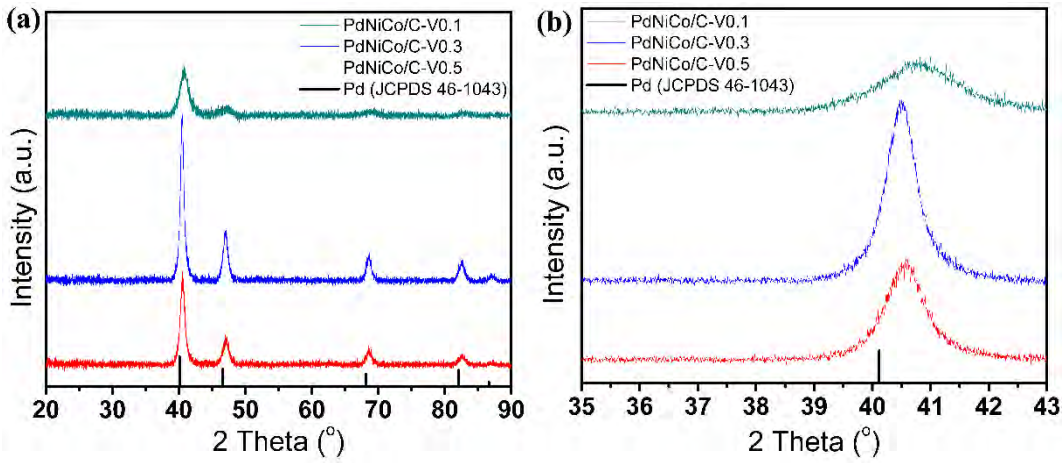

Figure 4.5 (a) XRD pattern and (b) Pd (111) of PdNiCo/C with different volume ratio

The effect of volume ratio does not show as peak shifted, but as peak broaden that can see in Figure 4.5 (b). The peak become narrow when the volume ratio decrease from 0.5 to 0.1. In addition, when the volume more decrease to 0.1, the peak become more broaden compare to the volume ratio 0.3. The same trend shows in grain size of catalyst that showed in Table 4.1. When the volume ratio decrease from 0.5 to 0.3, the grain size of catalyst increased from 12.0 to 13.6 nm. However, with more decrease the volume ratio to 0.1, the grain size is reducing to 7.7 nm. The results indicated that the decreasing volume of reducing agent would decrease the grain size of nanoparticle. Zhu et al. (Zhu et al., 2004) reported that the molar ratio of reducing agent to precursors determines the phase and size of nanoparticles influenced by reduction rate on the nucleation. At lower volume of reducing agent large grain size obtained, which indicated incomplete reduction of metal ions. At higher molar ratio of reducing agent, intramicelles nucleation and growth would promoted (Nandanwar et al., 2011).

Table 4.1 XRD result of PdNiCo/C with different volume ratio

Electrocatalysts	Peak Region	Peak Position	Grain Size (nm)
PdNiCo/C-V0.5	35-45°	40.570°	12.0
PdNiCo/C-V0.3	35-45°	40.473°	13.6
PdNiCo/C-V0.1	35-45°	40.992°	7.7

SEM images of PdNiCo/C with different volume ratio shown in Figure 4.6. The SE images show the particles formed a rounded structure and some of them were aggregated formed larger shape. The BSE images show the existence of catalyst particles in spherical and aggregate shape. The aggregate structure in PdNiCo/C are due to magnetic property of metal (Hou et al., 2005) and the van der Wall bonding of each particle (Wang and Tseng, 2009).

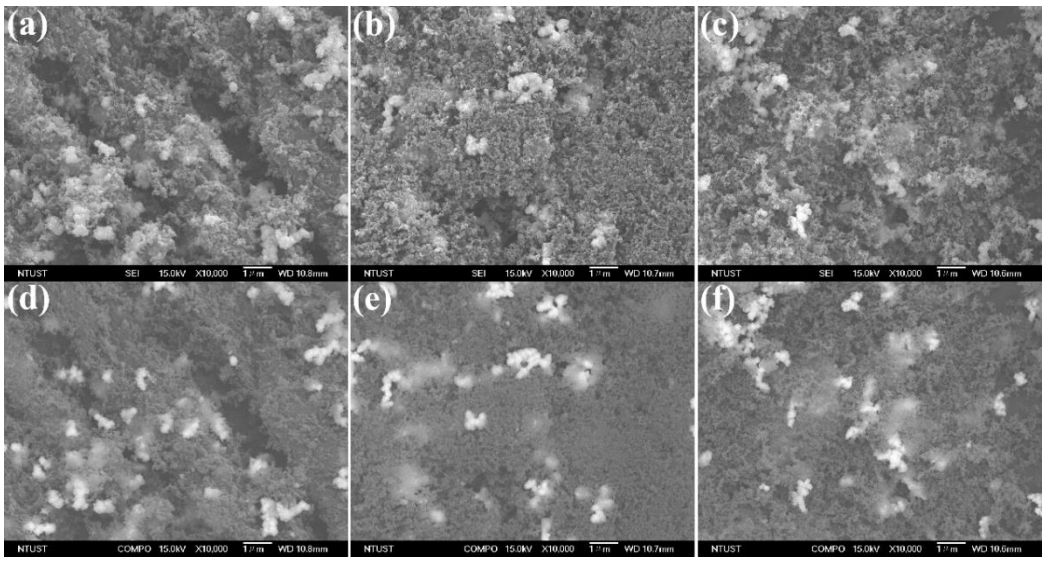

Figure 4.6 SEM images of (a) PdNiCo/C-V0.5, (b) PdNiCo/C-V0.3, and (c) PdNiCo/C-V0.1. The images (d), (e), and (f) are BSE images mode of PdNiCo/C-V0.5, PdNiCo/C-V0.3, and PdNiCo/C-V0.1, respectively

Figure 4.7 shows the CV curve of PdNiCo/C with different volume ratio. The CV taken in 1 M KOH solution with scan rate 50 mV s^{-1}. There are three clear peaks in the curve, in potential range from 0.1 to 0.5 V, 0.9 to 1.2 V, and 0.9 to

0.5 V (backward scan) that corresponding to adsorption OH- on the surface catalyst (Wang et al., 2014), generation of Pd (II) oxides (Ren et al., 2014), and reduction of Pd (II) oxides in potential range (Ren et al., 2014), respectively. The calculated ESCA from PdO reduction are 0.264, 0.252, and 0.361 cm^2 for PdNiCo/C-V0.5, PdNiCo/C-V0.3, and PdNiCo/C-V0.1, respectively. These results show same trend as the grain size result, that the larger grain size will have smaller ESCA. It is confirm that the grain size of nanoparticle will affected to the ESCA of electrocatalyst (Nesselberger et al., 2011).

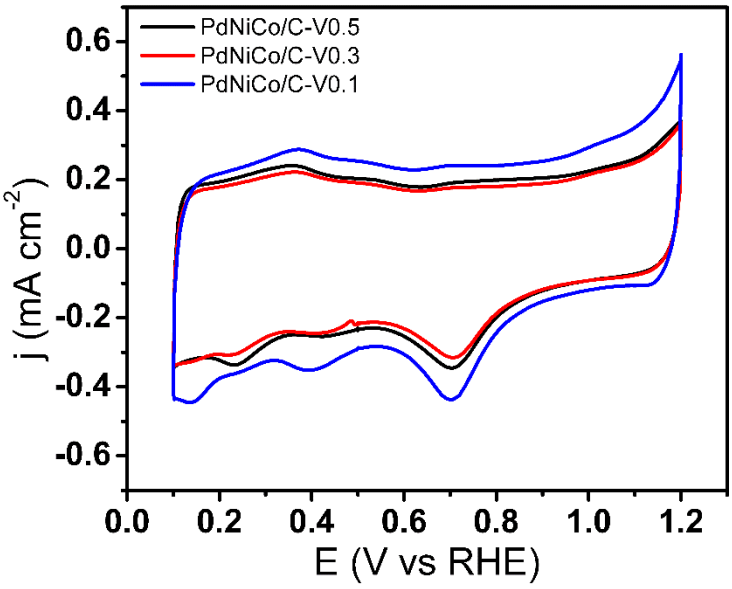

Figure 4.7 CV curve of PdNiCo/C with different volume ratio in 1 M KOH solution

The cyclic voltammogram of electrocatalysts toward MOR show in Figure 4.8 (a). It shows two large peaks that can be associate with the oxidation of freshly methanol and removal of carbonaceous species that not completely oxidize. Higher value of peak current density in the forward scan shows better electrocatalytic activity of the electrocatalysts for methanol oxidation. From the CV curve in methanol solution, it shows that PdNiCo/C-V0.9 has the higher current density in forward scan than that on other electrocatalysts. Figure 4.8 (b) shows the linear

sweep voltammetry (LSV) curve of PdNiCo/C with different volume ratio. The LSV shows the onset potential (defined at current density 0.5 mA cm^{-2}), the oxidation reaction begins to take place (Chen et al., 2015c). Comparing to the other catalysts that shown in the figure, PdNiCo/C-T150 shows the lowest onset potential. These two results (CV and LSV in 1 M KOH + 1 M methanol) indicates that the grain size and ESCA of electrocatalysts affected the electrocatalytic activity toward MOR. The smaller grain size and larger ESCA of electrocatalyst will get the better electrocatalytic activity towards MOR.

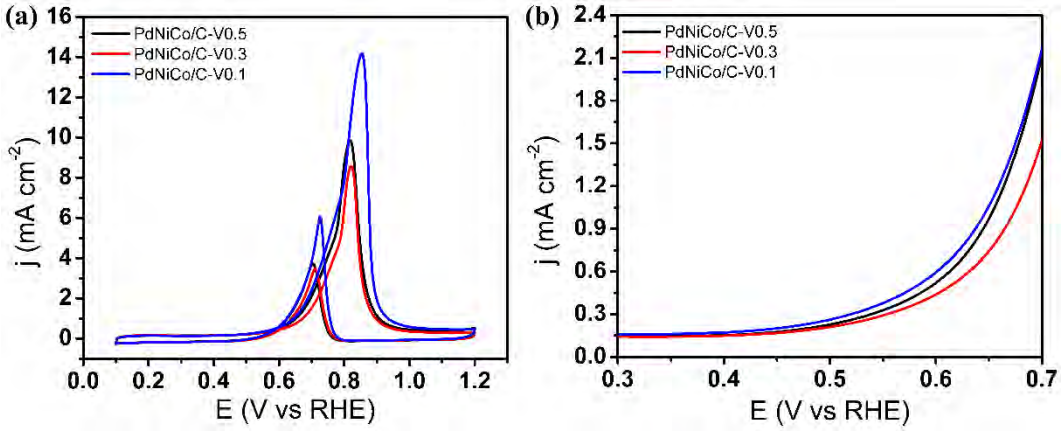

Figure 4.8 (a) CV and (b) LSV curves of PdNiCo/C with diffrent volume ratio agent in 1 M KOH + 1 M methanol solution

The results from this sub-chapter summarized in Table 4.2. It is shows that the PdNiCo/C with the temperature reduction at 150 ºC has best result. This because with higher reduction temperature, the grain size of nanoparticle become smaller which lead larger ESCA. Large ESCA of nanoparticle will lead better catalytic activity of electrocatalyst toward MOR which indicate by the peak of current density of CV and onset potential of LSV in 1 M KOH + 1 M methanol.

Table 4.2 Characteristic and Properties of PdNiCo/C with different volume ratio

Electrocatalysts	Grain Size (nm)	ESCA (cm^2)	Current Density Peak ($mA\ cm^{-2}$)	Onset Potential (V vs RHE)
PdNiCo/C-V0.5	12.0	0.264	9.85	0.60
PdNiCo/C-V0.3	13.6	0.252	8.55	0.61
PdNiCo/C-V0.1	7.7	0.552	14.17	0.58

4.2.2. Effect of Reduction Temperature on Properties of Catalyst

Reduction temperature of metal precursors will be affected the physical properties of nanoparticles. As shown in Figure 4.9 (a), there are peaks of Pd (111), (200), (220), and (311) in XRD pattern of PdNiCo/C. With addition of transition metal, the diffraction peaks of ternary alloy catalyst shift to higher 2θ values. As shown in Figure 4.9 (b), the 2θ of Pd (111) peak is slight shift to higher angle. The same trend replicated for Pd (200), Pd (220), and Pd (311) diffraction. This indicate a lattice contraction due to the substitution the nickel and cobalt atom in to FCC structure of Pd (Yang et al., 2010).

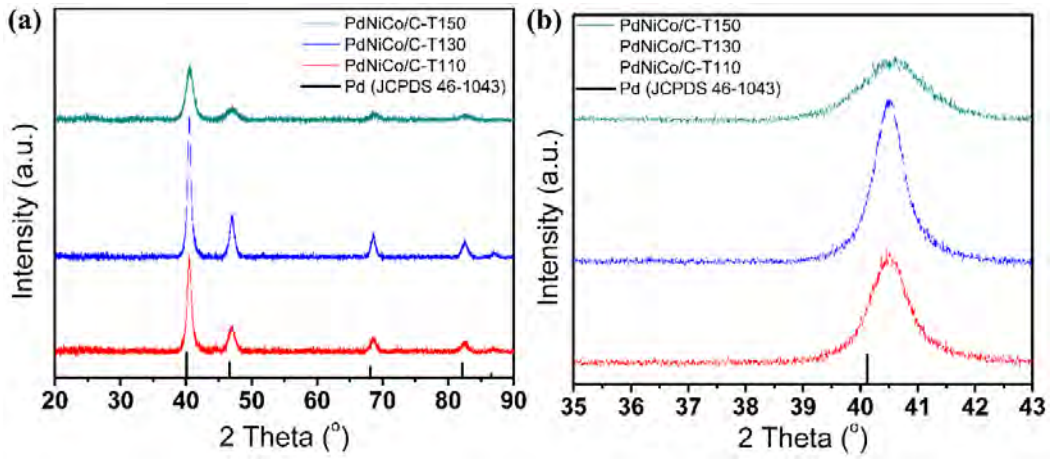

Figure 4.9 (a) XRD pattern and (b) Pd (111) of PdNiCo/C with different reduction temperature

The effect of reduction temperature shown as peak broaden that can see in Figure 4.9 (b). The peak become narrow when the temperature increase from 110 to 130 ºC. Moreover, when the temperature more increase to 150 ºC, the peak become more broaden compare to the 130 ºC. The same tren shows in grain size of catalyst that showed in Table 4.3. When the reduction temperature increase from 110 to 130 ºC, the grain size of catalyst also increased from 11.4 to 13.6 nm. However, with more increase the reduction temperature to 150 ºC, the grain size reduces to 8.9 nm. The reduction temperature was influenced the nucleation and the growth processes. At low temperature, the formation of nanoparticle consists of a reduction-nucleation stage, simultaneous reduction, nucleation, and growth stage and final growth stage. At higher temperature, the reduction, nucleation and growth process occurred simultaneously and very quickly (Sardar and Shumaker-Parry, 2011).

Table 4.3 XRD result of PdNiCo/C with different volume ratio

Electrocatalysts	Peak Region	Peak Position	Grain Size (nm)
PdNiCo/C-T110	35-45º	40.457	11.4
PdNiCo/C-T130	35-45º	40.472	13.6
PdNiCo/C-T150	35-45º	40.603	8.9

SEM images of PdNiCo/C with different reduction temperature shown in Figure 4.10. The SE images show the particles formed a rounded structure and some of them were aggregated formed larger shape. The BSE images show the existence of catalyst particles in spherical and aggregate shape. The aggregate structure in PdNiCo/C is due to magnetic property of metal (Hou et al., 2005) and the van der Wall bonding of each particle (Wang and Tseng, 2009).

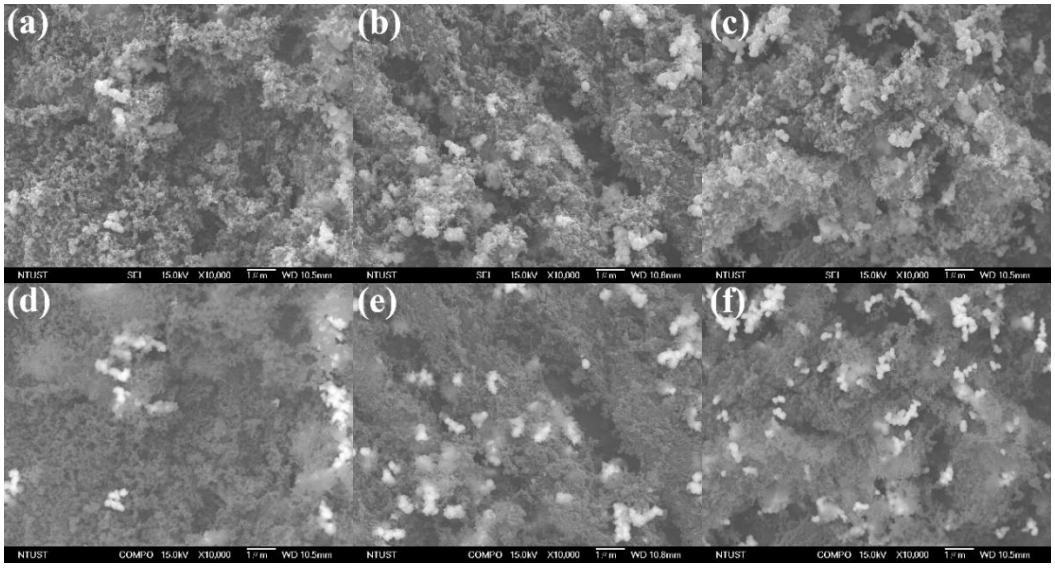

Figure 4.10 SEM images of (a) PdNiCo/C-T110, (b) PdNiCo/C-T130, and (c) PdNiCo/C-T150. The images (d), (e), and (f) are BSE images mode of PdNiCo/C-T110, PdNiCo/C-T130, and PdNiCo/C-T150, respectively

Figure 4.11 shows the CV curve of PdNiCo/C with different reduction temperature. The CV took in 1 M KOH solution with scan rate 50 mV s^{-1}. There are three clear peaks in the curve, in potential range from 0.1 to 0.5 V, 0.9 to 1.2, and 0.9 to 0.5 V which are corresponding to adsorption OH- on the surface catalyst (Wang et al., 2014), generation of Pd (II) oxides (Ren et al., 2014), and reduction of Pd (II) oxides (Ren et al., 2014), respectifully. The calculated ESCA from PdO reduction are 0.361, 0.264, and 0.552 cm^2 for PdNiCo/C-T110, PdNiCo/C-T130, and PdNiCo/C-T150, respectively. These results show same tren as the grain size result, that the larger grain size will have smaller ESCA. It is confirms that the grain size of nanoparticle will affected to the ESCA of electrocatalyst (Nesselberger et al., 2011).

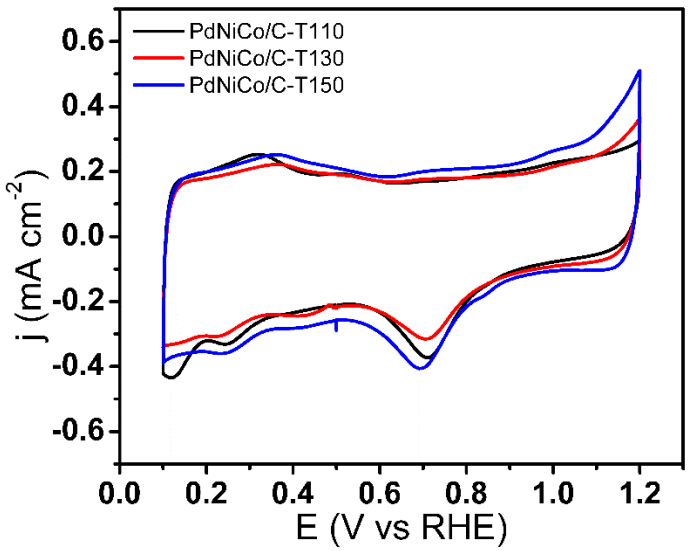

Figure 4.11 CV curve of PdNiCo/C with different reduction temperature in 1 M KOH solution

The cyclic voltammogram of electrocatalysts toward MOR show in Figure 4.12 (a). It shows two large peaks that can be associate with the oxidation of freshly methanol and removal of carbonaceous species that not completely oxidize. Higher value of peak current density in the forward scan shows better electrocatalytic activity of the electrocatalysts for methanol oxidation. From the CV curve in methanol solution, it shows that PdNiCo/C-T130 has the higher current density in forward scan than that on other electrocatalysts. Figure 4.12 (b) shows the linear sweep voltammetry (LSV) curve of PdNiCo/C with different volume ratio. The LSV shows the onset potential (defined at current density 0.5 mA cm^{-2}), the oxidation reaction begins to take place (Chen et al., 2015c). Comparing to the other catalysts that shown in the Figure 4.12 (b), PdNiCo/C-T130 shows the lowest onset potential. These two results (CV and LSV in 1 M KOH + 1 M methanol) indicates that the grain size and ESCA of electrocatalysts affected the electrocatalytic activity toward MOR. The smaller grain size and larger ESCA of electrocatalyst will get the better electrocatalytic activity towards MOR.

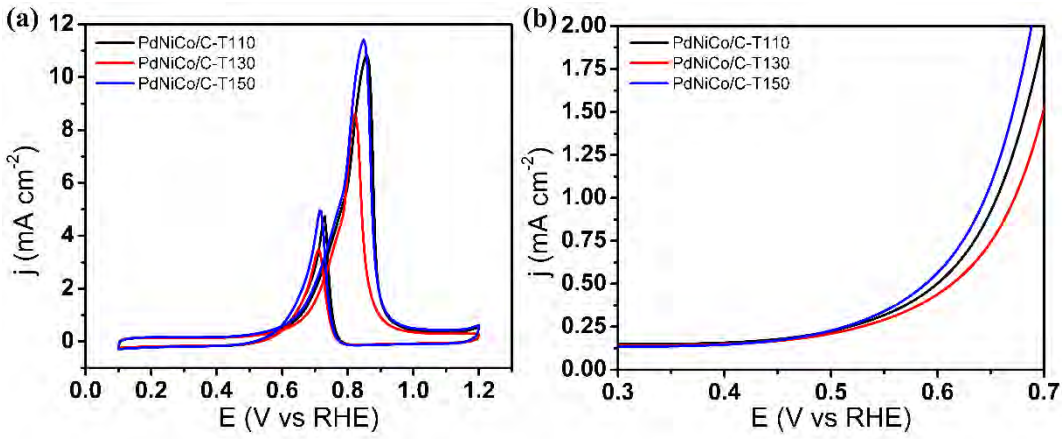

Figure 4.12 (a) CV and (b) LSV curves of PdNiCo/C with diffrent reduction temperature in 1 M KOH + 1 M methanol solution

The results from this sub-chapter are summarize in Table 4.4. It is shows that the PdNiCo/C with the reduction temperature is 150 ºC. This because with higher reduction temperature, the grain size of nanoparticles become smaller which lead larger ESCA. Large ESCA of nanoparticle will lead better catalytic activity of electrocatalyst toward MOR which indicate by the peak of current density of CV and onset potential of LSV in 1 M KOH + 1 M methanol.

Table 4.4 Characteristic and Properties of PdNiCo/C with different reduction temperature

Electrocatalysts	Grain Size (nm)	ESCA (cm^2)	Current Density Peak ($mA\ cm^{-2}$)	Onset Potential (V vs RHE)
PdNiCo/C-T110	11.4	0.361	10.81	0.59
PdNiCo/C-T130	13.6	0.264	8.57	0.61
PdNiCo/C-T150	8.9	0.362	11.41	0.59

4.2.3. PdNiCo/C with Best Synthesize Parameter

For more improve the catalytic activity toward MOR, PdNiCo/C synthesized by best volume ratio and reduction temperature. Volume ratio of

reduction to total volume and reduction temperature of metal precursors will be affected the physical properties of nanoparticles. As shown in Figure 4.13 (a), there are peaks of Pd (111), (200), (220), and (311) in XRD pattern of PdNiCo/C. With addition of transition metal, the diffraction peaks of ternary alloy catalyst shift to higher 2θ values due to addition of metal alloy. As shown in Figure 4.13 (b), the 2θ of Pd (111) peak is slight shift to higher angle, from 40.24° in Pd/C to 40.99°, 40.60°, and 40.66° in PdNiCo/C-V0.1, PdNiCo/C-T150, and PdNiCo/C-V0.1,T150, respectively. The same trend is replicate for Pd (200), Pd (220), and Pd (311) diffraction. This indicate a due to the substitution the nickel and cobalt atom in to FCC structure of Pd (Yang et al., 2010).

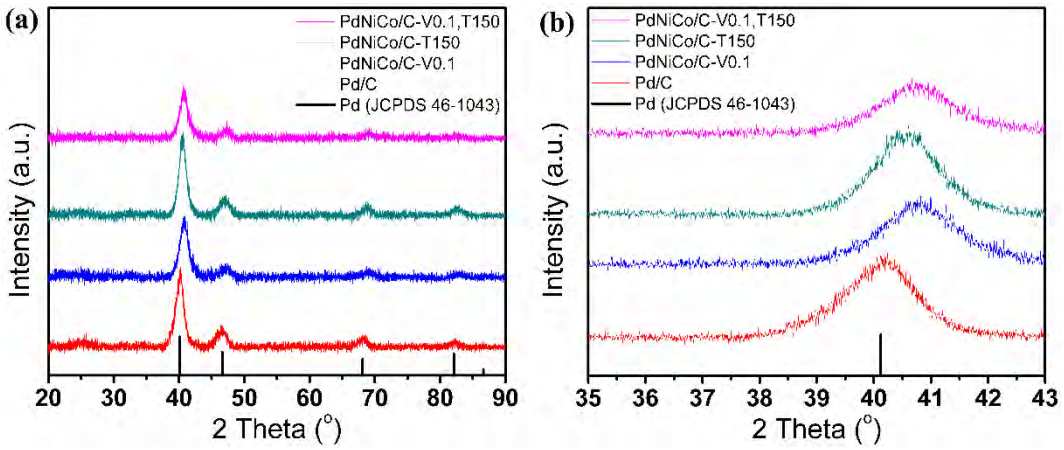

Figure 4.13 (a) XRD pattern and (b) Pd (111) of PdNiCo/C with different parameter

The effect of different parameters shows as peak broaden. The peak of PdNiCo/C-V0.1,T150 is most broaden compare to Pd/C and the other PdNiCo/C. The same trend shows in grain size of catalyst that showed in Table 4.5. The grain size of PdNiCo/C-V0.1,T150 catalyst has smaller grain size (7.34 nm). Zhu et al. (Zhu et al., 2004) reported that the molar ratio of reducing agent to precursors determines the phase and size of nanoparticles influenced by reduction rate on the nucleation. The reduction temperature was influenced the nucleation and the growth processes. At low temperature, the formation of nanoparticle consists of a

reduction-nucleation stage, simultaneous reduction, nucleation, and growth stage and final growth stage. At higher temperature, the reduction, nucleation and growth process occurred simultaneously and very quickly (Sardar and Shumaker-Parry, 2011). These two factors affected the grain size of nanoparticles. Lower volume ratio and reduction temperature lead to smaller nanoparticles.

Table 4.5 XRD result of PdNiCo/C

Electrocatalysts	Peak Region	Peak Position	Grain Size (nm)
Pd/C	35-45º	40.24	7.7
PdNiCo/C-V0.1	35-45º	40.99	7.7
PdNiCo/C-T150	35-45º	40.60	8.9
PdNiCo/C-V0.1,T150	35-45º	40.67	7.4

SEM images of Pd/C and PdNiCo/C with different parameters shows in Figure 4.14. The SE images show the particle formed a rounded structure and some of them were aggregated formed larger shape. The BSE images shows the existence of catalyst particles in spherical and aggregated shape. The causes of aggregate structured of PdNiCo/C almost similar with the Pd/C. the aggregate structure of Pd/C is due to van der Wall bonding of each particle (Wang and Tseng, 2009). However, the aggregate structure in PdNiCo/C is due also to magnetic property of metal (Hou et al., 2005).

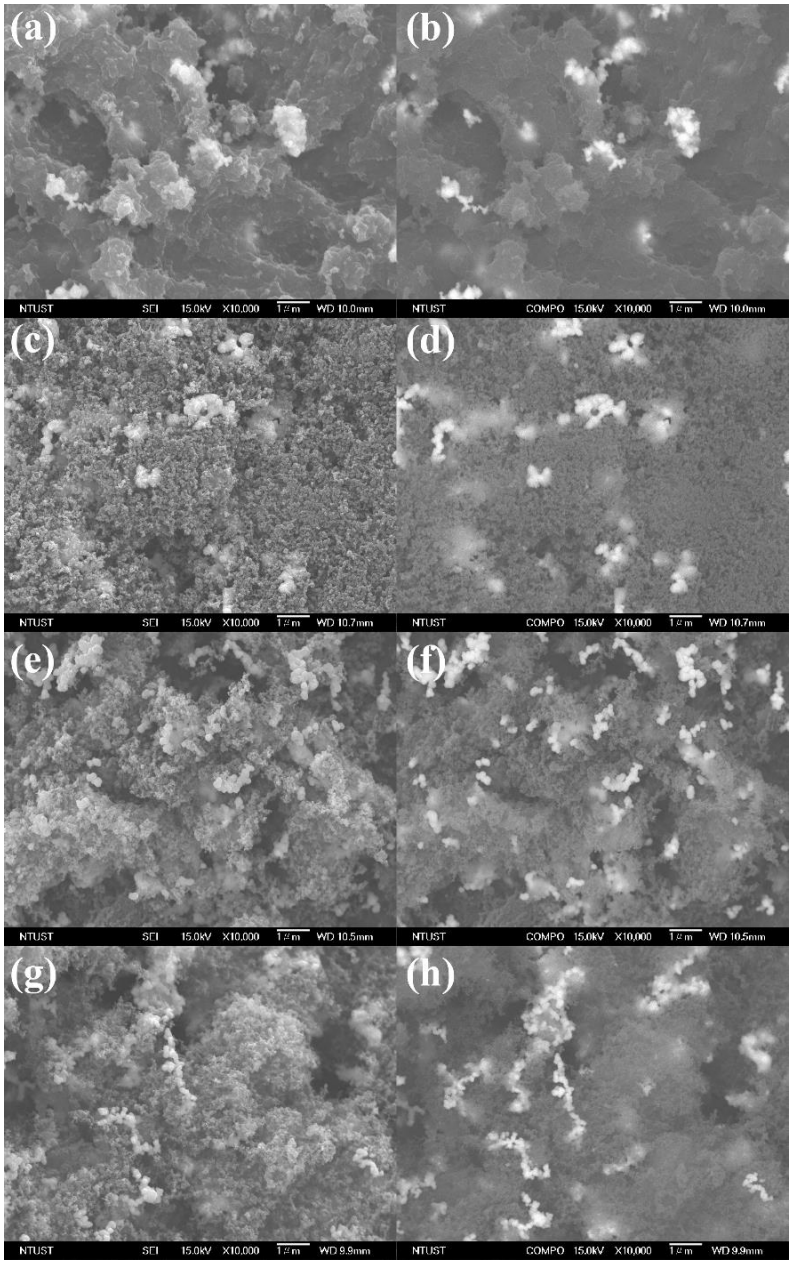

Figure 4.14 SEM images of (a) Pd/C, (b) PdNiCo/C-V0.1, (c) PdNiCo/C-T150, and (d) PdNiCo/C-V0.1,T150. The images (e), (f), (g), and (h) are BSE images mode of Pd/C, PdNiCo/C-V0.1, PdNiCo/C-T150, and PdNiCo/C-V0.1,T150, respectively

Figure 4.15 shows the CV curve of Pd/C and PdNiCo/C with different parameters. The CV took in 1 M KOH solution with scan rate 50 mV s^{-1}. There are three clear peaks in the curve, in potential range from 0.1 to 0.5 V, 0.9 to 1.2, and 0.9 to 0.5 V which are corresponding to adsorption OH- on the surface catalyst

(Wang et al., 2014), generation of Pd (II) oxides (Ren et al., 2014), and reduction of Pd (II) oxides (Ren et al., 2014), respectfully. Calculated ESCA from PdO reduction shows PdNiCo/C has the largest ESCA (0.5373 cm^2). This result is same as the grain size result, that the larger grain size will have smaller ESCA. It confirms that the grain size of nanoparticle will affected to the ESCA of electrocatalyst (Nesselberger et al., 2011).

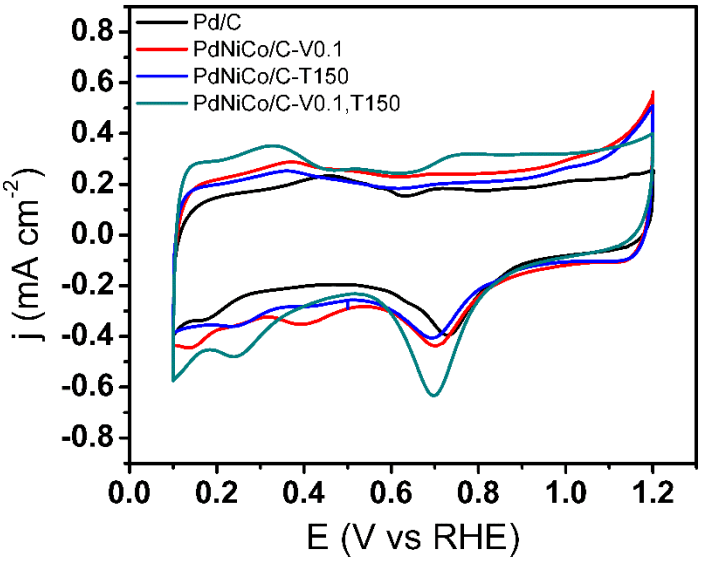

Figure 4.15 CV curve of PdNiCo/C with different parameter in 1 M KOH solution

The cyclic voltammogram of electrocatalysts toward MOR show in Figure 4.16 (a). It shows two large peaks that can be associate with the oxidation of freshly methanol and removal of carbonaceous species that not completely oxidize. Higher value of peak current density in the forward scan shows better electrocatalytic activity of the electrocatalysts for methanol oxidation. From the CV curve in methanol solution, it shows that PdNiCo/C-V0.1,T150 has the higher current density in forward scan than that on other electrocatalysts. Figure 4.16 (b) shows the linear sweep voltametry (LSV) curve of PdNiCo/C with different volume ratio. The LSV shows the onset potential (defined at current density 0.5 mA cm^{-2}), the oxidation reaction begins to take place (Chen et al., 2015c). Comparing to the other

catalysts that shown in the Figure 4.16 (b), PdNiCo/C-V0.1,T150 shows the lowest onset potential (0.57 V vs RHE). These two results (CV and LSV in 1 M KOH + 1 M methanol) indicates that the grain size and ESCA of electrocatalysts affected the electrocatalytic activity toward MOR. The smaller grain size and larger ESCA of electrocatalyst lead to the better electrocatalytic activity towards MOR.

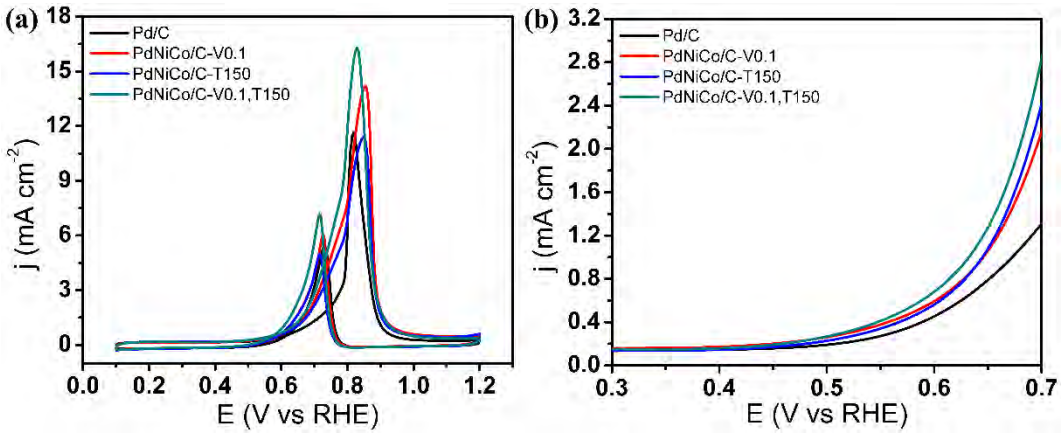

Figure 4.16 (a) CV and (b) LSV curves of PdNiCo/C with diffrent parameter in 1 M KOH + 1 M methanol solution

The results from this sub-chapter are summarize in Table 4.6. It is shows that the PdNiCo/C with. This because with higher reduction temperature, the grain size of nanoparticle become smaller which lead larger ESCA. Large ESCA of nanoparticle will lead better catalytic activity of electrocatalyst toward MOR which indicate by the peak of current density of CV and onset potential of LSV in 1 M KOH + 1 M methanol.

Table 4.6 Characteristic and Properties of PdNiCo/C

Electrocatalysts	Grain Size (nm)	ESCA (cm^2)	Current Density Peak (mA cm^{-2})	Onset Potential (V vs RHE)
Pd/C	7.7	0.446	11.64	0.61
PdNiCo/C-V0.1	7.7	0.552	14.17	0.58
PdNiCo/C-T150	8.9	0.362	11.41	0.59
PdNiCo/C-V0.1,T150	7.4	0.573	16.32	0.57

4.3. Effect of Different Alloying Elements on Catalytic Activity of Electrocatalyst

Each element has different catalytic properties towards MOR. When some elements alloying to form a new type of electrocatalyst, their catalytic activity will change. In this sub-chapter, effect of different alloying elements in ternary alloy electrocatalyst on physical properties and catalytic activity studied. The main catalyst in this alloy is palladium, and the alloying elements are nickel, iron, and cobalt. To study their characteristic, PdNiCo/C, PdFeCo, and PdNiFe/C was prepared.

Figure 4.17 (a) shows XRD pattern of Pd/C and ternary alloy electrocatalysts with different alloying elements. There are no distinguish peak of Ni, Fe or Co, which suggests the formation of a solid solution between the metal alloys (Sieben et al., 2014). All ternary alloy electrocatalysts show peak shifted to higher angel compare to that on Pd/C. Pd (111) peak is located at 40.24 in Pd/C. but it shifted to higher angle to 40.66º, 40.92º, and 40.67º in PdNiCo/C, PdFeCo/C and PdNiFe/C, respectively. Same trend also applied for Pd (200), (220), and (311). Theses peak shift is attribute to substitution of elements into FCC structure of Pd.

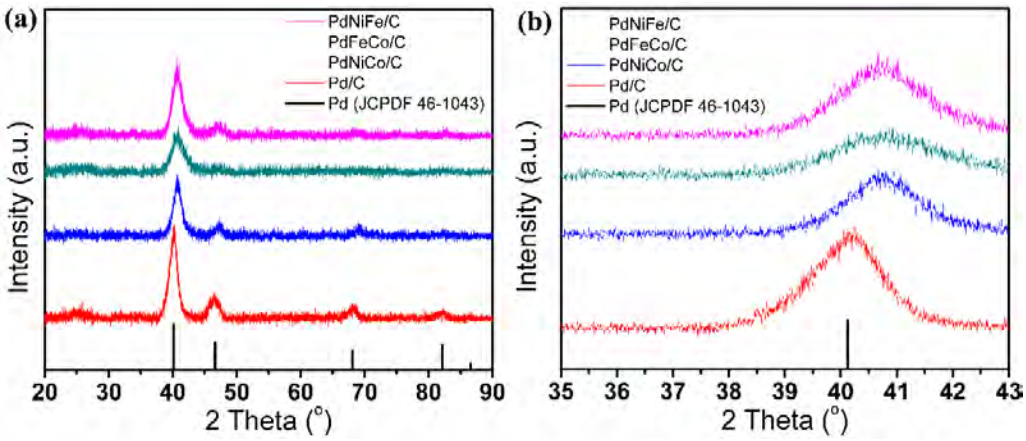

Figure 4.17 (a) XRD pattern and (b) Pd (111) of PdNiCo/C with different alloying elements

The grain size of electrocatalyst is calculated using equation (3.1). The grain size of catalysts is 7.7, 7.4, 6.9 and 7.1 nm for Pd/C, PdNiCo/C, PdFeCo/C, PdNiFe/C, respectively. Same average size of electrocatalysts will make the measurement of catalytic activity of catalyst depend on alloying elements. The lattice, as shown in parameter of Pd/C, PdNiCo/C, PdFeCo/C, and PdNiFe/C is 0.2239, 0.2216, 0.2202, and 0.2215, respectively. The incorporation of metal alloys, which has smaller atom, into the Pd lattice resulted in a lattice parameter contraction that leading to the decrease in lattice parameter.

Figure 4.10 shows TEM images of Pd/C and Pd-based ternary alloy. The TEM images shows particle formed a rounded structure and some of them were aggregated formed larger shape. The aggregate structure in PdNiCo/C is due to magnetic property of metal (Hou et al., 2005) and the van der Wall bonding of each particle (Wang and Tseng, 2009).

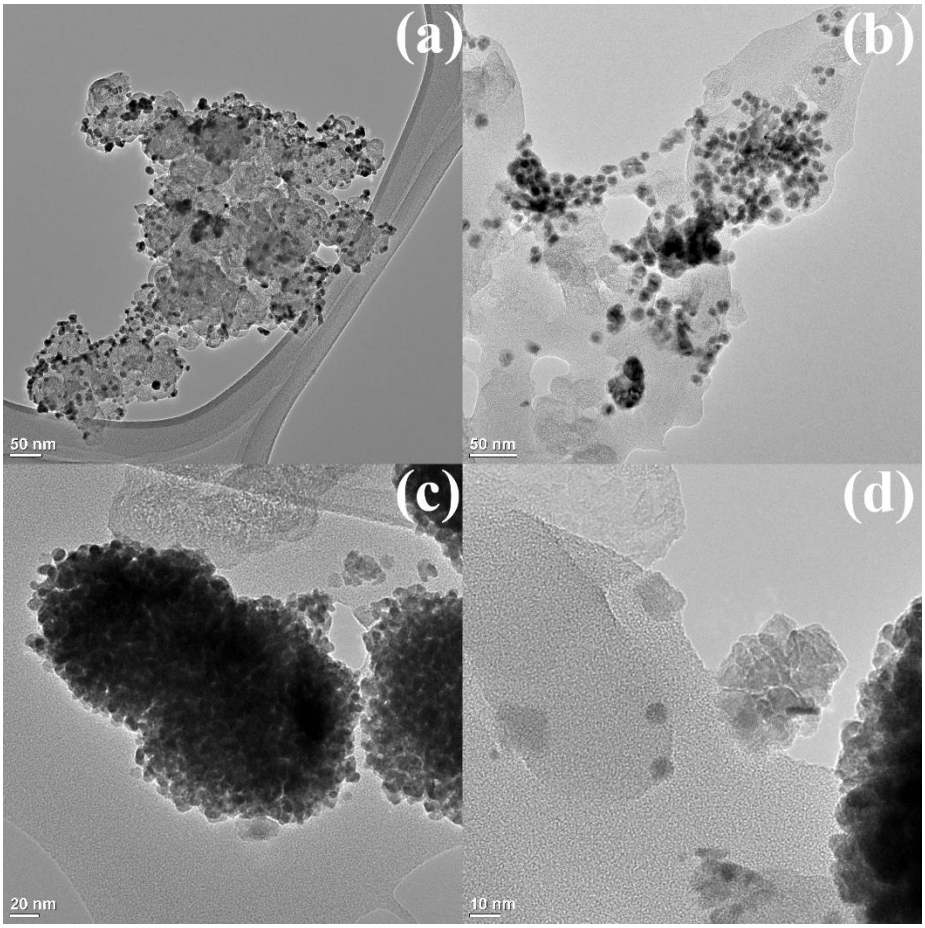

Figure 4.18 TEM images of (a) Pd/C, (b) PdNiCo/C, (c) PdFeCo/C, and (d) PdNiFe/C

Figure 4.19 shows the HRTEM images and selected area electron diffraction (SAED) pattern of Pd/C and Pd-base ternary alloy electrocatalysts. The lattice parameter of Pd/C that shows in HRTEM image is 0.224 nm. Compared to the Pd/C, the Pd-based ternary alloy electrocatalysts have smaller lattice parameter. The lattice parameter for PdNiCo/C, PdFeCo/C, PdNiFe/C are 0.222, 0.222, and 0.220 nm, respectively. Although there are little different in diameter value, all SAED pattern show same diffraction ring that associated to Pd (111), Pd (200), Pd (220), and Pd (311) These results are in agreement with XRD analysis, considering standard deviation.

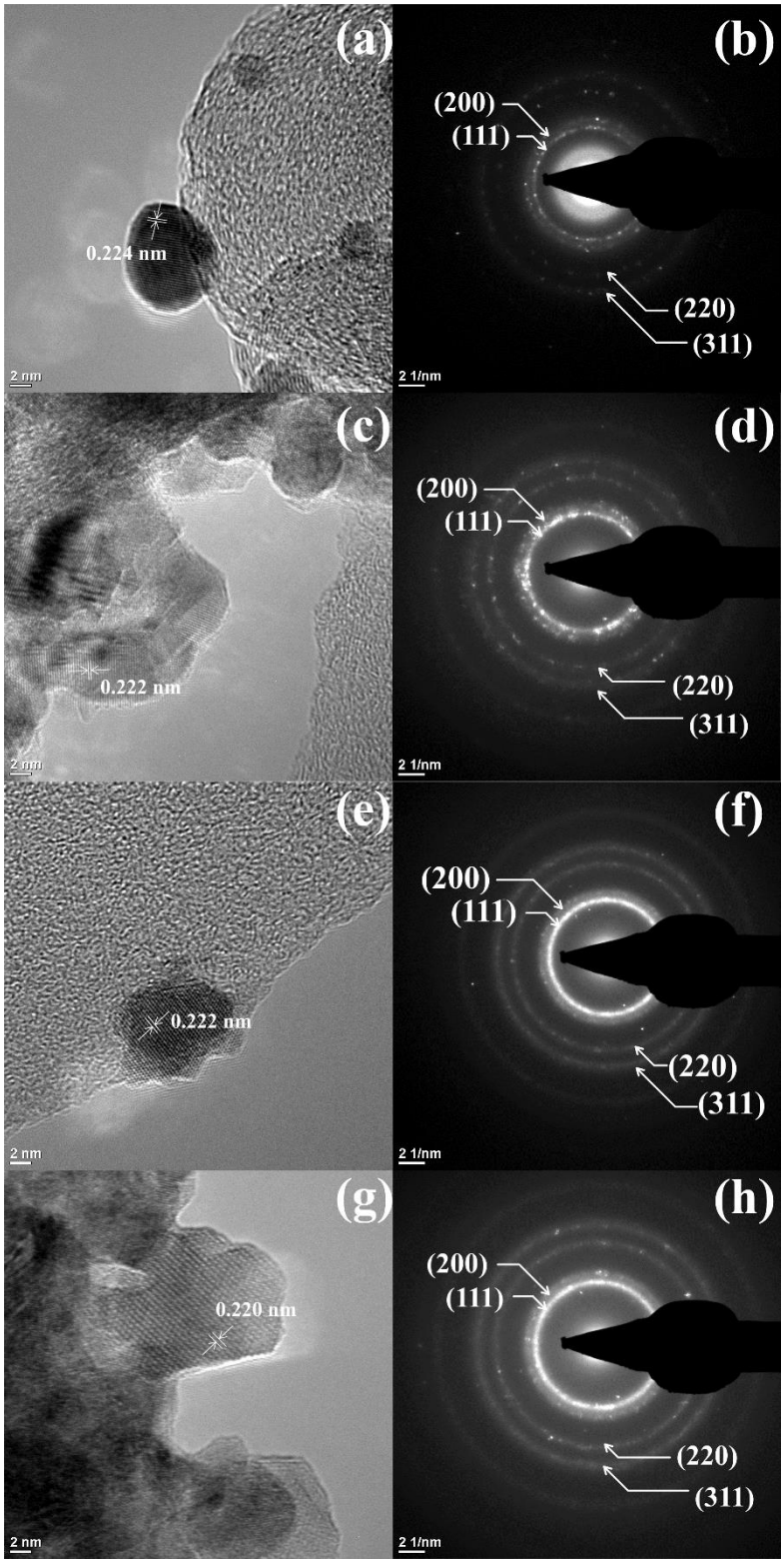

Figure 4.19 HRTEM images with inset shows SAED pattern of (a)(b) Pd/C, (c)(d) PdNiCo/C, (f)(e) PdFeCo/C, and (g)(h) PdNiFe/C

Table 4.7 Grain size and lattice parameter as-prepared electrocatalysts

Electrocatalysts	Grain Size (nm)	Lattice Parameter from XRD (nm)	Lattice Parameter from SAED (nm)
Pd/C	7.7	0.2240	0.224
PdNiCo/C	7.4	0.2215	0.222
PdFeCo/C	6.9	0.2216	0.222
PdNiFe/C	7.1	0.2203	0.220

Figure 4.20 shows the CV curve of Pd/C and Pd-base ternary alloy. The CV taken in 1 M KOH solution with scan rate 50 mV s^{-1}. There are three clear peaks in the curve, in potential range from 0.1 to 0.5 V, 0.9 to 1.2 V, and 0.9 to 0.5 V (backward scan) that corresponding to adsorption OH- on the surface catalyst (Wang et al., 2014), generation of Pd (II) oxides (Ren et al., 2014), and reduction of Pd (II) oxides in potential range (Ren et al., 2014), respectively. The calculated ESCA from PdO reduction region are 0.446, 0.573, 0.804, and 0.733 cm^2 for Pd/C, PdNiCo/C, PdFeCo/C, and PdNiFe/C, respectively.

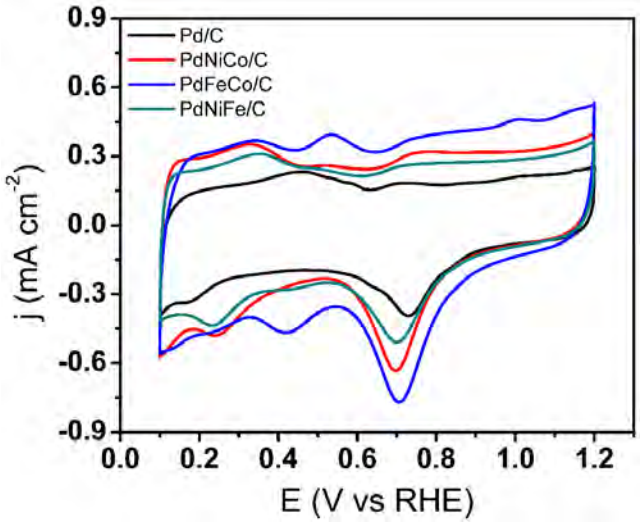

Figure 4.20 CV curve in 1 M KOH of electrocatalyst with different alloying elements

The cyclic voltammogram of electrocatalysts toward MOR shown in Figure 4.21 (a). It shows two large peaks that can be associate with the oxidation of freshly methanol and removal of carbonaceous species that not completely oxidize. Higher value of peak current density in the forward scan shows better electrocatalytic activity of the electrocatalysts for methanol oxidation (Chen et al., 2015c). From the CV curve in methanol solution and Table 4.8, it shows that PdFeCo/C has the higher current density in forward scan than that on other electrocatalysts. Figure 4.21 (b) shows the linear sweep voltammetry (LSV) curve of Pd/C and Pd-based ternary alloy. The LSV shows the onset potential (defined at current density 0.5 mA cm^{-2}), the oxidation reaction begins to take place (Chen et al., 2015c). Comparing to the other catalysts that shown in the Table 4.8, PdFeCo/C shows the lowest onset potential. These two results (CV and LSV in 1 M KOH + 1 M methanol) indicates that ESCA and type of element of electrocatalysts affected the electrocatalytic activity toward MOR.

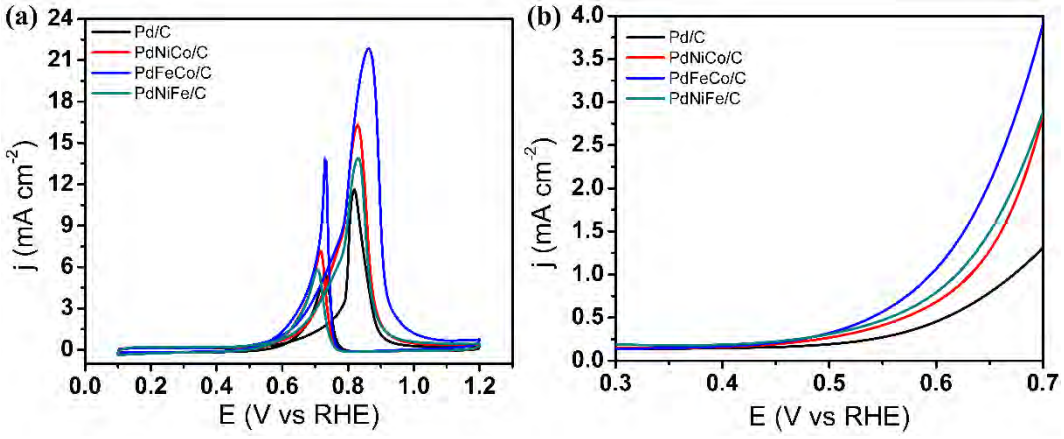

Figure 4.21 CV curve in 1 M KOH + 1 M methanol of electrocatalyst with different alloying elements

Figure 4.22 show the chronoamperogram of Pd/C and Pd-based ternary alloy electrocatalysts. Chronoamperometry conducted to study the stability of electrocatalysts. PdFeCo/C shows the highest current density after 3600 s (Table

4.8) than that on other electrocatalyst. With highest current density, PdFeCo/C more suitable as electrocatalyst for DMFC application.

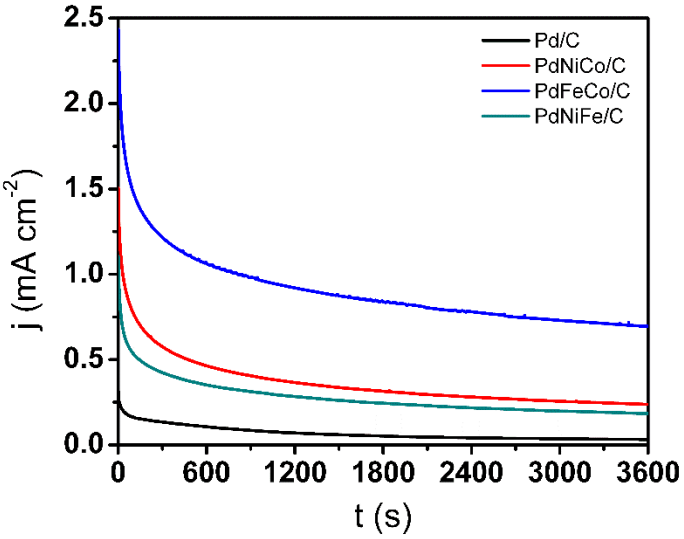

Figure 4.22 CA curve in 1 M KOH +1 M methanol of electrocatalyst with different alloying elements

Table 4.8 ESCA in 1 M KOH and catalytic activity in 1 M KOH + 1 M methanol of Pd/C and Pd-based ternary alloy electrocatalysts

Electrocatalysts	ESCA (cm^2)	Peak Current Density (mA cm^{-2})	Onset Potential (V vs RHE)	Current Density at 3600 s (mA cm^{-2})
Pd/C	0.446	11.64	0.61	0.03
PdNiCo/C	0.573	16.32	0.57	0.24
PdFeCo/C	0.804	21.84	0.54	0.69
PdNiFe/C	0.733	13.89	0.56	0.18

CHAPTER V
CONCLUSIONS

In this study, effect of volume ratio between reducing agent and total volume, and reduction temperature was conducted to improve the catalytic activity. Volume ratio 0.1 and reducing temperature 150 ºC was found has best catalytic activity toward MOR. SEM images shows that the electrocatalyst formed a round structure and some of them are aggregated. By increasing the volume ratio, the grain size of elctrocatalysts become smaller. This result was found in PdNiCo/C-V0.1, which had grain size 7.7 nm. Smaller grain size, lead the PdNiCo/C-V0.1 had larger ESCA (0.552 cm^2) and good catalytic activity toward MOR that showed with high current density (14.17 mA cm^{-2}) and low onset potential (0.58 V vs RHE).

The higher reduction temperature, would lead the grain size also became smaller. PdNiCo/C-T150 had smaller grain size, 8.9 nm. Smaller grain size would lead the electrocatalysts have larger ESCA (0.362 cm^2). Large ESCA leads the electrocatalysts have more active sites. The larger active site would help the catalysts to better oxidize the methanol that indicate by high current density (11.41 mA cm^{-2}) and low onset potential (0.57 V vs RHE).

By combining this two best parameter, PdNiCo/C-V0.1,T150 was synthesized. It showed decrase in grain size to 7.4 nm. Decreased in grain size, leading to increasing ESCA value to 0.573 cm^2. PdNiCo/C-V0.1,T150 had current density peak in MOR at 16.32 mA cm^{-2} and onset potential at 0.57 V vs RHE.

To study the effect of different alloying elements, Pd/C, PdNiCo/C, PdFeCo/C and PdNiFe/C was synthesized. PdFeCo/C showed smallest grain size, followed by PdNiFe/C, PdNiCo/C, and Pd/C. In terms of ESCA, PdFeCo/C showed the largest one, followed by PdNiFe/C, PdNiCo/C, and Pd/C. The catalytic activity toward MOR showed that PdFeCo/C was the best one. PdFeCo/C had peak current density at 21.84 mA cm^{-2} and onset potential at 0.54 V vs RHE. Based on stability,

PdFeCo/C maintain at high current density compared to other electrocatalyst. The current density of PdFeCo/C after 3600 s was 0.69 mA cm^{-2}.

REFERENCES

Amin, R. S., Abdel Hameed, R. M., El-Khatib, K. M. & Elsayed Youssef, M. 2014. Electrocatalytic activity of nanostructured Ni and Pd-Ni on Vulcan XC-72R carbon black for methanol oxidation in alkaline medium. *International Journal of Hydrogen Energy,* 39**,** 2026-2041.

Antolini, E. & Gonzalez, E. R. 2010. Alkaline direct alcohol fuel cells. *Journal of Power Sources,* 195**,** 3431-3450.

Arikan, T., Kannan, A. M. & Kadirgan, F. 2013. Binary Pt-Pd and ternary Pt-Pd-Ru nanoelectrocatalysts for direct methanol fuel cells. *International Journal of Hydrogen Energy,* 38**,** 2900-2907.

Baglio, V., D'urso, C., Sebastian, D., Stassi, A. & Arico, A. S. PtCo catalyst with modulated surface characteristics for the cathode of direct methanol fuel cells. 2014. Elsevier Ltd, 5399-5405.

Barakat, N. A. M., Abdelkareem, M. A., Yousef, A., Al-Deyab, S. S., El-Newehy, M. & Kim, H. Y. 2013. Cadmium-doped cobalt/carbon nanoparticles as novel nonprecious electrocatalyst for methanol oxidation. *International Journal of Hydrogen Energy,* 38**,** 3387-3394.

Chen, D.-J., Zhang, Q.-L., Feng, J.-X., Ju, K.-J., Wang, A.-J., Wei, J. & Feng, J.-J. 2015a. One-pot wet-chemical co-reduction synthesis of bimetallic gold-platinum nanochains supported on reduced graphene oxide with enhanced electrocatalytic activity. *Journal of Power Sources,* 287**,** 363-369.

Chen, M., Lou, B., Ni, Z. & Xu, B. 2015b. PtCo nanoparticles supported on expanded graphite as electrocatalyst for direct methanol fuel cell. *Electrochimica Acta,* 165**,** 105-109.

Chen, W., Zhang, Y. & Wei, X. 2015c. Catalytic performances of PdNi/MWCNT for electrooxidations of methanol and ethanol in alkaline media. *International Journal of Hydrogen Energy,* 40**,** 1154-1162.

Cho, Y.-H., Kim, O.-H., Chung, D. Y., Choe, H., Cho, Y.-H. & Sung, Y.-E. 2014. PtPdCo ternary electrocatalyst for methanol tolerant oxygen reduction

reaction in direct methanol fuel cell. *Applied Catalysis B: Environmental,* 154-155**,** 309-315.

Choi, S.-I., Xie, S., Shao, M., Odell, J. H., Lu, N., Peng, H.-C., Protsailo, L., Guerrero, S., Park, J., Xia, X., Wang, J., Kim, M. J. & Xia, Y. 2013. Synthesis and characterization of 9 nm Pt-Ni octahedra with a record high activity of 3.3 A/mgPt for the oxygen reduction reaction. *Nano Letters,* 13**,** 3420-3425.

Chu, Y.-Y., Wang, Z.-B., Jiang, Z.-Z., Gu, D.-M. & Yin, G.-P. 2012. Facile synthesis of hollow spherical sandwich PtPd/C catalyst by electrostatic self-assembly in polyol solution for methanol electrooxidation. *Journal of Power Sources,* 203**,** 17-25.

Chu, Y. Y., Wang, Z. B., Cao, J., Gu, D. M. & Yin, G. P. 2013. Ultrahigh durable PtPd/C nanowire networks catalyst synthesized by modified phase transfer method for methanol oxidation. *Fuel Cells,* 13**,** 380-386.

Fashedemi, O. O., Miller, H. A., Marchionni, A., Vizza, F. & Ozoemena, K. I. 2015. Electro-oxidation of ethylene glycol and glycerol at palladium-decorated FeCo@Fe core-shell nanocatalysts for alkaline direct alcohol fuel cells: Functionalized MWCNT supports and impact on product selectivity. *Journal of Materials Chemistry A,* 3**,** 7145-7156.

Gervasio, D. 2009. FUEL CELLS – DIRECT ALCOHOL FUEL CELLS | New Materials A2 - Garche, Jürgen. *Encyclopedia of Electrochemical Power Sources.* Amsterdam: Elsevier.

Hartnig, C. 2012. 3 - Catalyst and membrane technology for low temperature fuel cells. *Polymer Electrolyte Membrane and Direct Methanol Fuel Cell Technology.* Woodhead Publishing.

Hou, Y., Kondoh, H., Shimojo, M., Sako, E. O., Ozaki, N., Kogure, T. & Ohta, T. 2005. Inorganic nanocrystal self-assembly via the inclusion interaction of -cyclodextrins: Toward 3D spherical magnetite. *Journal of Physical Chemistry B,* 109**,** 4845-4852.

Hsieh, C.-T. & Lin, J.-Y. 2009. Fabrication of bimetallic Pt-M (M = Fe, Co, and Ni) nanoparticle/carbon nanotube electrocatalysts for direct methanol fuel cells. *Journal of Power Sources,* 188**,** 347-352.

Hung, C.-T., Liou, Z.-H., Veerakumar, P., Wu, P.-H., Liu, T.-C. & Liu, S.-B. 2016. Ordered mesoporous carbon supported bifunctional PtM (M = Ru, Fe, Mo) electrocatalysts for a fuel cell anode. *Chinese Journal of Catalysis,* 37**,** 43-53.

Jang, H. D., Kim, S. K., Chang, H., Choi, J.-H., Cho, B.-G., Jo, E. H., Choi, J.-W. & Huang, J. 2015. Three-dimensional crumpled graphene-based platinum-gold alloy nanoparticle composites as superior electrocatalysts for direct methanol fuel cells. *Carbon,* 93**,** 869-877.

Jeon, M. K., Zhang, Y. & Mcginn, P. J. 2009. Effect of reduction conditions on electrocatalytic activity of a ternary PtNiCr/C catalyst for methanol electro-oxidation. *Electrochimica Acta,* 54**,** 2837-2842.

Ji, Z., Shen, X., Zhu, G., Chen, K., Fu, G. & Tong, L. 2012. Enhanced electrocatalytic performance of Pt-based nanoparticles on reduced graphene oxide for methanol oxidation. *Journal of Electroanalytical Chemistry,* 682**,** 95-100.

Jin, X., He, B., Miao, J., Yuan, J., Zhang, Q. & Niu, L. 2012. Stabilization and dispersion of PtRu and Pt nanoparticles on multiwalled carbon nanotubes using phosphomolybdic acid, and the use of the resulting materials in a direct methanol fuel cell. *Carbon,* 50**,** 3083-3091.

Jorissen, L. & Gogel, V. 2009. FUEL CELLS - DIRECT ALCOHOL FUEL CELLS | Direct Methanol: Overview A2 - Garche, Jürgen. *Encyclopedia of Electrochemical Power Sources.* Amsterdam: Elsevier.

Kakati, N., Maiti, J., Jee, S. H., Lee, S. H. & Yoon, Y. S. 2011. Hydrothermal synthesis of PtRu on CNT/SnO2 composite as anode catalyst for methanol oxidation fuel cell. *Journal of Alloys and Compounds,* 509**,** 5617-5622.

Kakati, N., Maiti, J., Lee, S. H. & Yoon, Y. S. 2012. Core shell like behavior of PdMo nanoparticles on multiwall carbon nanotubes and their methanol oxidation activity in alkaline medium. *International Journal of Hydrogen Energy,* 37**,** 19055-19064.

Kim, J. H., Kwon, S. Y., Bhattacharjya, D., Chai, G. S. & Yu, J.-S. 2013. High-performance quaternary PtRuIrNi electrocatalysts with hierarchical nanostructured carbon support. *Journal of Catalysis,* 306**,** 133-145.

Kim, T., Kobayashi, K., Take, T. & Nagai, M. 2012. Electronic modification effects induced by Fe in Pt-Ru-Fe ternary catalyst on the electrooxidation of CO/H2 and methanol. *Journal of Oleo Science,* 61**,** 127-134.

La-Torre-Riveros, L., Guzman-Blas, R., Mendez-Torres, A. E., Prelas, M., Tryk, D. A. & Cabrera, C. R. 2012. Diamond nanoparticles as a support for Pt and PtRu catalysts for direct methanol fuel cells. *ACS Applied Materials and Interfaces,* 4**,** 1134-1147.

Lee, K., Kang, S. W., Lee, S.-U., Park, K.-H., Lee, Y. W. & Han, S. W. 2012. One-pot synthesis of monodisperse 5 nm Pd-Ni nanoalloys for electrocatalytic ethanol oxidation. *ACS Applied Materials and Interfaces,* 4**,** 4208-4214.

Li, R., Mao, H., Zhang, J., Huang, T. & Yu, A. 2013. Rapid synthesis of porous Pd and PdNi catalysts using hydrogen bubble dynamic template and their enhanced catalytic performance for methanol electrooxidation. *Journal of Power Sources,* 241**,** 660-667.

Li, W., Zhao, X. & Manthiram, A. 2014. Room-temperature synthesis of Pd/C cathode catalysts with superior performance for direct methanol fuel cells. *Journal of Materials Chemistry A,* 2**,** 3468-3476.

Liu, H., Song, C., Zhang, L., Zhang, J., Wang, H. & Wilkinson, D. P. 2006. A review of anode catalysis in the direct methanol fuel cell. *Journal of Power Sources,* 155**,** 95-110.

Liu, J., Cao, L., Huang, W. & Li, Z. 2012. Direct electrodeposition of PtPd alloy foams comprised of nanodendrites with high electrocatalytic activity for the oxidation of methanol and ethanol. *Journal of Electroanalytical Chemistry,* 686**,** 38-45.

Liu, M., Peng, C., Yang, W., Guo, J., Zheng, Y., Chen, P., Huang, T. & Xu, J. 2015. Pd nanoparticles supported on three-dimensional graphene aerogels as highly efficient catalysts for methanol electrooxidation. *Electrochimica Acta,* 178**,** 838-846.

Liu, Z., Su, F., Zhang, X. & Tay, S. W. 2011. Preparation and characterization of PtRu nanoparticles supported on nitrogen-doped porous carbon for electrooxidation of methanol. *ACS Applied Materials and Interfaces,* 3**,** 3824-3830.

Lu, Y., Jiang, Y., Wu, H. & Chen, W. 2013. Nano-PtPd cubes on graphene exhibit enhanced activity and durability in methanol electrooxidation after CO stripping-cleaning. *Journal of Physical Chemistry C,* 117**,** 2926-2938.

Luo, B., Yan, X., Xu, S. & Xue, Q. 2013. Synthesis of worm-like PtCo nanotubes for methanol oxidation. *Electrochemistry Communications,* 30**,** 71-74.

Lv, J.-J., Li, S.-S., Wang, A.-J., Mei, L.-P., Chen, J.-R. & Feng, J.-J. 2014a. Monodisperse Au-Pd bimetallic alloyed nanoparticles supported on reduced graphene oxide with enhanced electrocatalytic activity towards oxygen reduction reaction. *Electrochimica Acta,* 136**,** 521-528.

Lv, Q., Xiao, Y., Yin, M., Ge, J., Xing, W. & Liu, C. 2014b. Reconstructed PtFe alloy nanoparticles with bulk-surface differential structure for methanol oxidation. *Electrochimica Acta,* 139**,** 61-68.

Ma, L., Chu, D. & Chen, R. 2012. Comparison of ethanol electro-oxidation on Pt/C and Pd/C catalysts in alkaline media. *International Journal of Hydrogen Energy,* 37**,** 11185-11194.

Maiyalagan, T., Wang, X. & Manthiram, A. 2014. Highly active Pd and Pd-Au nanoparticles supported on functionalized graphene nanoplatelets for enhanced formic acid oxidation. *RSC Advances,* 4**,** 4028-4033.

Mancharan, R. & Goodenough, J. B. 1992. Methanol oxidation in acid on ordered NiTi. *Journal of Materials Chemistry,* 2**,** 875-887.

Manthiram, A., Zhao, X. & Li, W. 2012. 11 - Developments in membranes, catalysts and membrane electrode assemblies for direct methanol fuel cells (DMFCs). *Functional Materials for Sustainable Energy Applications.* Woodhead Publishing.

Mikkelsen, K., Cassidy, B., Hofstetter, N., Bergquist, L., Taylor, A. & Rider, D. A. 2014. Block copolymer templated synthesis of core-shell PtAu bimetallic nanocatalysts for the methanol oxidation reaction. *Chemistry of Materials,* 26**,** 6928-6940.

Nandanwar, S. U., Chakraborty, M. & Murthy, Z. V. P. 2011. Formation of ruthenium nanoparticles by the mixing of two reactive microemulsions. *Industrial and Engineering Chemistry Research,* 50**,** 11445-11451.

Nassr, A. B. A. A., Sinev, I., Grunert, W. & Bron, M. 2013. PtNi supported on oxygen functionalized carbon nanotubes: In depth structural characterization and activity for methanol electrooxidation. *Applied Catalysis B: Environmental,* 142-143**,** 849-860.

Nassr, A. B. A. A., Sinev, I., Pohl, M.-M., Grunert, W. & Bron, M. 2014. Rapid microwave-assisted polyol reduction for the preparation of highly active PtNi/CNT electrocatalysts for methanol oxidation. *ACS Catalysis,* 4**,** 2449-2462.

Nesselberger, M., Ashton, S., Meier, J. C., Katsounaros, I., Mayrhofer, K. J. J. & Arenz, M. 2011. The particle size effect on the oxygen reduction reaction activity of Pt catalysts: Influence of electrolyte and relation to single crystal models. *Journal of the American Chemical Society,* 133**,** 17428-17433.

Ozturk, Z., Sen, F., Sen, S. & Gokagac, G. 2012. The preparation and characterization of nano-sized Pt-Pd/C catalysts and comparison of their superior catalytic activities for methanol and ethanol oxidation. *Journal of Materials Science,* 47**,** 8134-8144.

Qin, Y.-L., Liu, Y.-C., Liang, F. & Wang, L.-M. 2015. Preparation of Pd-Co-based nanocatalysts and their superior applications in formic acid decomposition and methanol oxidation. *ChemSusChem,* 8**,** 260-263.

Qiu, H. & Huang, X. 2012. Nanoporous PtFe surface alloy architecture for enhanced methanol electro-oxidation. *Journal of Materials Chemistry,* 22**,** 7602-7608.

Qiu, H. & Zou, F. 2012. Nanoporous PtCo surface alloy architecture with enhanced properties for methanol electrooxidation. *ACS Applied Materials and Interfaces,* 4**,** 1404-1410.

Ren, F., Zhai, C., Zhu, M., Wang, C., Wang, H., Bin, D., Guo, J., Yang, P. & Du, Y. 2015. Facile synthesis of PtAu nanoparticles supported on polydopamine reduced and modified graphene oxide as a highly active catalyst for methanol oxidation. *Electrochimica Acta,* 153**,** 175-183.

Ren, Y., Zhang, S. & Li, H. 2014. Electro-oxidation of methanol on SnO2-promoted Pd/MWCNTs catalysts in alkaline solution. *International Journal of Hydrogen Energy,* 39**,** 288-296.

Renjith, A. & Lakshminarayanan, V. 2015. One step preparation of 'ready to use' Au@Pd nanoparticle modified surface using deep eutectic solvents and a study of its electrocatalytic properties in methanol oxidation reaction. *Journal of Materials Chemistry A,* 3**,** 3019-3028.

Salazar-Banda, G. R., Eguiluz, K. I. B., Pupo, M. M. S., Suffredini, H. B., Calegaro, M. L. & Avaca, L. A. 2012. The influence of different co-catalysts in Pt-based ternary and quaternary electro-catalysts on the electro-oxidation of methanol and ethanol in acid media. *Journal of Electroanalytical Chemistry,* 668**,** 13-25.

Sardar, R. & Shumaker-Parry, J. S. 2011. Spectroscopic and microscopic investigation of gold nanoparticle formation: Ligand and temperature effects on rate and particle size. *Journal of the American Chemical Society,* 133**,** 8179-8190.

Scofield, M. E., Koenigsmann, C., Wang, L., Liu, H. & Wong, S. S. 2015. Tailoring the composition of ultrathin, ternary alloy PtRuFe nanowires for the methanol oxidation reaction and formic acid oxidation reaction. *Energy and Environmental Science,* 8**,** 350-363.

Sieben, J. M., Alvarez, A. E., Comignani, V. & Duarte, M. M. E. 2014. Methanol and ethanol oxidation on carbon supported nanostructured Cu core Pt-Pd shell electrocatalysts synthesized via redox displacement. *International Journal of Hydrogen Energy,* 39**,** 11547-11556.

Singh, R. N., Madhu & Awasthi, R. 2013. Chapter 16 - Alcohol Fuel Cells A2 - Suib, Steven L. *New and Future Developments in Catalysis.* Amsterdam: Elsevier.

Singh, R. N., Singh, A. & Anindita 2009. Electrocatalytic activity of binary and ternary composite films of Pd, MWCNT and Ni, Part II: Methanol electrooxidation in 1 M KOH. *International Journal of Hydrogen Energy,* 34**,** 2052-2057.

Su, Y. K., Liu, H., Feng, M., Yan, Z. L., Cheng, Z. H., Tang, J. N. & Yang, H. T. 2015. Bimetallic Pt3Co nanowires as electrocatalyst: The effects of thermal treatment on electrocatalytic oxidation of Methanol. *Electrochimica Acta,* 161**,** 124-128.

Vegard, L. 1921. Die Konstitution der Mischkristalle und die Raumfüllung der Atome. *Zeitschrift für Physik,* 5**,** 17-26.

Wang, D.-Y., Chou, H.-L., Lin, Y.-C., Lai, F.-J., Chen, C.-H., Lee, J.-F., Hwang, B.-J. & Chen, C.-C. 2012. Simple replacement reaction for the preparation of ternary Fe 1-xPtRux nanocrystals with superior catalytic activity in methanol oxidation reaction. *Journal of the American Chemical Society,* 134**,** 10011-10020.

Wang, R., Wang, H., Wei, B., Wang, W. & Lei, Z. 2010. Carbon supported Pt-shell modified PdCo-core with electrocatalyst for methanol oxidation. *International Journal of Hydrogen Energy,* 35**,** 10081-10086.

Wang, R., Wu, Z., Wang, G., Qin, Z., Chen, C., Dong, M., Zhu, H., Fan, W. & Wang, J. 2015. Highly active Au-Pd nanoparticles supported on three-dimensional graphene-carbon nanotube hybrid for selective oxidation of methanol to methyl formate. *RSC Advances,* 5**,** 44835-44839.

Wang, S.-R. & Tseng, W. J. 2009. Aggregate structure and crystallite size of platinum nanoparticles synthesized by ethanol reduction. *Journal of Nanoparticle Research,* 11**,** 947-953.

Wang, Y., Wang, Y., Zang, J., Dong, L., Pan, H. & Yuan, Y. 2013. Graphitized nanodiamond supporting PtNi alloy as stable anodic and cathodic electrocatalysts for direct methanol fuel cell. *Electrochimica Acta,* 113**,** 583-590.

Wang, Y., Zhao, Y., Yin, J., Liu, M., Dong, Q. & Su, Y. 2014. Synthesis and electrocatalytic alcohol oxidation performance of Pd-Co bimetallic nanoparticles supported on graphene. *International Journal of Hydrogen Energy,* 39**,** 1325-1335.

Winterbone, D. E. & Turan, A. 2015. Chapter 21 - Fuel Cells. *Advanced Thermodynamics for Engineers (Second Edition).* Boston: Butterworth-Heinemann.

Wu, Y.-N., Liao, S.-J., Guo, H.-F. & Hao, X.-Y. 2013. Preparation of high-performance PdPt-Pt core-shell catalyst with shortened carbon nanotubes as support. *Journal of Power Sources,* 235**,** 135-141.

Xia, T., Shen, H., Chang, G., Zhang, Y., Shu, H., Oyama, M. & He, Y. 2014. Facile and rapid synthesis of ultrafine ptpd bimetallic nanoparticles and their high performance toward methanol electrooxidation. *Journal of Nanomaterials,* 2014.

Xiang, D. & Yin, L. 2012. Well-dispersed and size-tuned bimetallic PtFex nanoparticle catalysts supported on ordered mesoporous carbon for enhanced electrocatalytic activity in direct methanol fuel cells. *Journal of Materials Chemistry,* 22**,** 9584-9593.

Xu, C., Wang, L., Mu, X. & Ding, Y. 2010. Nanoporous PtRu alloys for electrocatalysis. *Langmuir,* 26**,** 7437-7443.

Yang, J., Cheng, C. H., Zhou, W., Lee, J. Y. & Liu, Z. 2010. Methanol-tolerant heterogeneous PdCo@PdPt/C electrocatalyst for the oxygen reduction reaction. *Fuel Cells,* 10**,** 907-913.

Yang, Y., Wang, L., Li, A., Jia, Z., Wang, Y. & Qi, T. 2015. Novel palladiumyttrium (PdY/C) catalysts for methanol electrooxidation in alkaline media. *Journal of Solid State Electrochemistry,* 19**,** 923-927.

Yin, Z., Lin, L. & Ma, D. 2014. Construction of Pd-based nanocatalysts for fuel cells: Opportunities and challenges. *Catalysis Science and Technology,* 4**,** 4116-4128.

Yu, E. H., Krewer, U. & Scott, K. 2010. Principles and materials aspects of direct alkaline alcohol fuel cells. *Energies,* 3**,** 1499-1528.

Zhang, J., Yang, H., Fang, J. & Zou, S. 2010. Synthesis and Oxygen Reduction Activity of Shape-Controlled Pt3Ni Nanopolyhedra. *Nano Letters,* 10**,** 638-644.

Zhang, X., Guan, P., Malic, L., Trudeau, M., Rosei, F. & Veres, T. 2015a. Nanoporous twinned PtPd with highly catalytic activity and stability. *Journal of Materials Chemistry A,* 3**,** 2050-2056.

Zhang, X., Zhang, B., Liu, D. & Qiao, J. 2015b. One-pot synthesis of ternary alloy CuFePt nanoparticles anchored on reduced graphene oxide and their enhanced electrocatalytic activity for both methanol and formic acid oxidation reactions. *Electrochimica Acta,* 177**,** 93-99.

Zhang, X., Zhang, Y.-C., Zhang, J.-W. & Zhang, B. 2015c. Anchoring ternary CuFePd nanocatalysts on reduced graphene oxide to improve the electrocatalytic activity for the methanol oxidation reaction. *RSC Advances,* 5**,** 101563-101568.

Zhang, Y., Gu, Y.-E., Lin, S., Wei, J., Wang, Z., Wang, C., Du, Y. & Ye, W. 2011. One-step synthesis of PtPdAu ternary alloy nanoparticles on graphene with superior methanol electrooxidation activity. *Electrochimica Acta,* 56**,** 8746-8751.

Zhao, T. S. & Xu, C. 2009. FUEL CELLS – DIRECT ALCOHOL FUEL CELLS | Direct Methanol Fuel Cell: Overview Performance and Operational Conditions A2 - Garche, Jürgen. *Encyclopedia of Electrochemical Power Sources.* Amsterdam: Elsevier.

Zhao, Y., Fan, L., Ren, J. & Hong, B. 2014. Electrodeposition of Pt-Ru and Pt-Ru-Ni nanoclusters on multi-walled carbon nanotubes for direct methanol fuel cell. *International Journal of Hydrogen Energy,* 39**,** 4544-4557.

Zhu, F., Ma, G., Bai, Z., Hang, R., Tang, B., Zhang, Z. & Wang, X. 2015. High activity of carbon nanotubes supported binary and ternary Pd-based catalysts for methanol, ethanol and formic acid electro-oxidation. *Journal of Power Sources,* 242**,** 610-620.

Zhu, H.-T., Zhang, C.-Y. & Yin, Y.-S. 2004. Rapid synthesis of copper nanoparticles by sodium hypophosphite reduction in ethylene glycol under microwave irradiation. *Journal of Crystal Growth,* 270**,** 722-728.

BIOGRAPHY

Yusuf Pradesar was born in Surabaya (Indonesia) at February 21st 1992. He is first son of Pranowo Sidi and Ade Dewi Sartika. He got his bachelor degree of engineering from Materials and Metallurgical Engineering ITS Indonesia. His final project for bachelor degree was "**Effect of Ultrasonication Time and Holding Time of Hydrothermal Process on Structure and Electrical Properties of Graphene Material**". He took master degree in Materials and Metallurgical Engineering ITS. He got opportunity for pursuit double degree program in Taiwan. Therefore, he also studied in Materials Science and Engineering NTUST Taiwan. When study in NTUST, he doing a reaseach about fuel cell. He got his master degree with the thesis title "**Pd-based Ternary Alloy Supported Carbon Black with High Methanol Oxidation Reaction for Direct Methanol Fuel Cell**".